Influence of partial shear connection on the behaviour of U-shaped steel concrete beams with L-shaped shear connectors

C. Lepourry-Nicollet, P. Heng, H. Somja, F. Palas

INFLUENCE OF PARTIAL SHEAR CONNECTION ON THE BEHAVIOUR OF U-SHAPED STEEL CONCRETE BEAMS WITH L-SHAPED SHEAR CONNECTORS

Clemence Lepourry-Nicollet[a, b], Piseth Heng[a,*], Hugues Somja[a], Franck Palas[c]

[a] *Université Européenne de Bretagne – INSA Rennes, LGCGM/ Structural Engineering Research Group , 20 avenue des Buttes de Coësmes, CS 70839, F-35708 Rennes Cedex 7, France*

[b] *INGENOVA, Civil Engineering Office, 5 Rue Louis Jacques Daguerre, 35136 Saint-Jacques-de-la-Lande, France*

[c] *Concept Technique Design R & D, 89 Boulevard de Laval, 35500 Vitré, France*

[*] Corresponding author: piseth.heng@insa-rennes.fr

Abstract

This paper presents a study on the influence of partial shear connection on the behaviour of the U-shaped steel concrete beams (USCB) with L-shaped shear connectors. An experimental campaign of three full-scale experimental tests on the USCB with a degree of shear connection ranging from 0.4 to 1 has been conducted under sagging bending moment. The test results showed high ductility of the USCB with both full and partial shear connections. The failure mode of the USCB was governed by the plastic buckling of the upper flanges of the U-shaped steel profile at the location of the shear connectors. The plastic moment resistance of the USCB with partial shear connection predicted by the full plastic analysis approach and by the simplified approach in Eurocode 4 agreed well with the experimental results. Furthermore, the flexural stiffness of the USCB with partial connections predicted by American and Australian standards fit well with the experimental results. A numerical model based on the two-layer beam element formulation taking into account the interlayer slips with continuous connection in a co-rotational framework was also adapted to determine the behaviour of the USCB. This model was validated against experimental tests as well as against the analytical approaches. It was finally used to carry out a parametrical study in order to investigate the effect of selected parameters such as the degree of shear connection, the concrete strength and the steel strength of U-shaped profile.

Keywords: Partial shear connection, L-shaped shear connector, U-shaped steel concrete beam, Flexural tests under sagging bending moment, two-layer beam element formulation.

1. Introduction

Over the past years, many forms of composite beams have been proposed in order to achieve the challenging architectural demand for long-span structures such as bridges and commercial buildings. In the so-called reinforced concrete beam, the inclusion of embedded steel rebars is needed for withstanding axial tensile stresses from flexural load whereas the concrete works well to resist to axial compressive stresses. However, the RC beam is not

efficient for longer spanned and tall structures due to its massive cross-section. The pre-fabricated pre-stressed concrete beams have been an alternative solution to achieve larger span-to-depth ratios, but their weight makes the handling expensive. In the same way, the detailing of the anchorage and the specific skills needed to introduce the tensioning force in the structure make post-tensioning beams complex and expensive. On the other hand, composite steel-concrete beams can reach suitable span-to-depth ratios while avoiding these inconveniences. Among other configurations, steel-concrete composite beams incorporating cold-form U-shaped steel profile as a permanent formwork have been intensively proposed in previous studies [1]-[7]. This new configuration of beams provides many advantages over traditional reinforced concrete beams such as more ductility, increases in shear capacities, higher span-to-depth ratio, and reduction in creep and shrinkage. The composite beams are usually composed of a steel beam, a reinforced concrete beam or slab, and shear connectors. The structural behaviour of the composite beams depends largely on the shear capacities of the connectors to transfer horizontal shear force between the steel and the concrete parts of the beams. The shear capacities can be contributed by three main sources at the interface between the steel and the concrete: chemical bonding, friction (depending on the roughness of the surfaces), and mechanical shear connection (embossments, ribs or shear connectors). The design of the shear connection can be categorized as full shear connection or partial shear connection. In the full shear connection design, sufficient strength is ensured at the steel-concrete interface, allowing the weaker between the concrete and the steel component to reach its strength. On the other hand, the maximum flexural shear capacity of the composite beams in the partial shear connection is governed by the failure at the steel-concrete interface before the full capacity of the steel or concrete beam is reached.

In most cases of medium-to-large span structures, the design is limited by the serviceability limit state requirements, i.e. the deflection limit. In such cases, the design using partial shear connection is more economical and preferable to that using full shear connection due to a substantial reduction of the number of shear connectors. Many studies in the past were conducted to determine the effect of the partial shear connection on the flexural behaviour of the popular I-shaped steel concrete composite beams with shear studs [8]-[11] and with channel type connectors [12][13]. Oehlers et al [9] distinguished the difference between the partial interaction and the partial shear connection and studied the effect of partial interaction on the full-shear connection strength of an I-profile steel concrete composite beam. On the other hand, Nie et al [11] performed 13 experimental tests on simply supported steel-concrete composite beams subjected to positive and negative bending moments with the degree of shear connection ranging from 0.25 to 1.85. By comparing their test results with the calculations based on the equivalent method provided in Eurocode 4 [14] and AISC [15], it was shown that partial shear connections could be used in both positive and negative bending regions for continuous composite beams with good accuracy. Baran and Topkaya [12] were interested in investigating the behaviour of steel-concrete partially composite beams with channel type shear connectors by performing single point bending tests on four composite beams with various degrees of connection. It was revealed that major improvement on moment capacity and stiffness was obtained even for beams with relatively low degree of partial shear connection, and that the moment inertia specified in AISC [15] specification overestimated the measured flexural stiffness of the beams for all degrees of partial degrees of connection investigated.

While U-shaped steel-concrete composite beams are considered as an interesting solution for long-span structures, their behaviour under the effect of partial shear interaction is still not well established. Among the few studies, Liu et al [6] performed bending tests on ten specimens of rebar stiffened cold-formed U-shaped steel-

concrete composite beams considering three parameters, among which is the degree of shear connection. The shear connection in their study was ensured by a rebar truss welded to top flanges of the U profile, shear stud and tensile reinforcement. It was found out that the ultimate bending capacity of the beams could be calculated according to Eurocode 4 [14] with the consideration of three modification factors in order to take into account for effective width of the slab, effective depth of steel web and the actual concrete compressive strength. However, the effect of partial shear connection on the behaviour of the composite beams itself was not fully investigated, except that it was grossly concluded that the increase of bending capacity was less than 10 percent by improving the degree of shear connection. Liu et al [5] studied the flexural behaviour of steel-concrete composite beams consisting of U-shaped steel girders and angle connectors by conducting four-point bending tests on five specimens with different connector intervals and installation locations, giving the degrees of shear connection ranging from 0.55 to 1. The results showed that the beam with angle connectors welded to the top flanges performed better than with angle connectors welded to the interior webs. Furthermore, they found that the ultimate flexural capacity of the fully composite beams could be reasonably estimated by the calculations following Eurocode 4 [14] and AISC [15] codes. Acceptable results of the ultimate bending capacity were also obtained for the partially composite beams using Eurocode 4 [14].

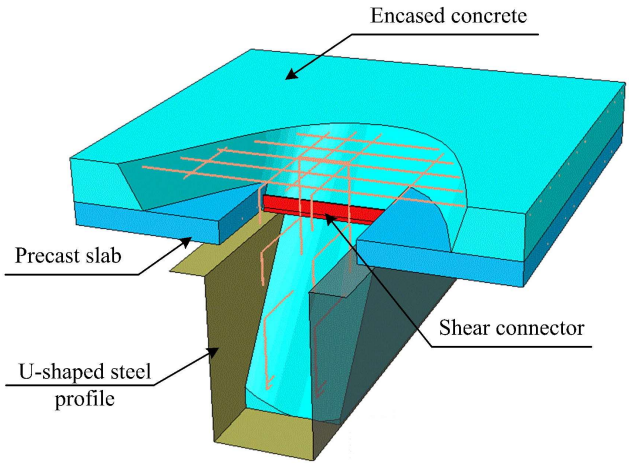

Figure 1: Configuration of U-shaped steel-concrete beams (USCB).

In a previous investigation by the authors [7], a configuration of U-shaped steel-concrete beams (USCB) with L-shaped shear connectors was proposed. The composite beam is composed of a U-shaped steel profile, precast and cast-in-place slabs, encased dropdown reinforced concrete beam and L-shaped connectors welded to top flanges of the U profile, as shown in Figure 1. In this configuration, the L-shaped connectors are fully embedded in the concrete, being functional also in limiting the uplifts. As the behaviour of this new type of shear connection is not covered yet in the current norms, the first study on its behaviour and on its force transfer mechanism was carried out through five asymmetrical push-out tests. The results were used to validate a complete 3D FE model of the test, which was then used for performing a parametric study in order to propose a design formula to predict the shear capacity of the shear connectors.

The next phase of the study presented in this article is needed to verify the performance of these shear connectors in the composite beams under positive bending moment considering partial shear connection. Three full-scale flexural tests on the USCB with a degree of shear connection ranging from 0.4 to 1 have been performed under

sagging bending moment in order to determine the moment resisting capacity, the slip distribution along the length of the beam, the strain distribution in the cross-section, the ductility, and the failure mode. Experimental results such as the moment resisting capacity and the flexural stiffness were then compared with the values predicted by different design approaches and standards. A numerical model based on the two-layer beam element formulation taking into account the interlayer slips with continuous connection in a co-rotational framework was also adopted to determine the behaviour of the USCB and validated against experimental tests as well as against the analytical approaches. At last, a parametrical study was carried out in order to investigate the effect of selected parameters such as the degree of shear connection, the concrete strength and the steel strength of the U-shaped profile.

2. Recall of asymmetrical pushout tests on L-shaped shear connectors in the USCB

A study on the behaviour of L-shaped shear connectors used in the USCB was previously performed by the authors through five large-scale pushout tests [7]. The tests were to quantify the strength and the deformation capacities of shear connectors as well as to gain an insight into the force transfer mechanism in the USCB. In the tests, the specimen was placed horizontally on two vertical supports connected with slotted holes and greased PTFE plates to allow displacements (see Figure 2). The pushout force was applied through the force jack to one end of the U-shaped steel beam, whereas the opposite end surface of the concrete slab was put in contact with a rigid beam that blocked the displacement of the specimen, giving the reaction against the pushout force. A total of four tests are recalled here. The first specimen denoted by PO-L40 has three connectors with L-shaped section of 40×40×4mm. The last three specimens denoted by PO-L50a, PO-L50b and PO-L50c have three connectors with L-shaped section of 50×50×5mm. These connectors were welded on the top flanges of the U-profile.

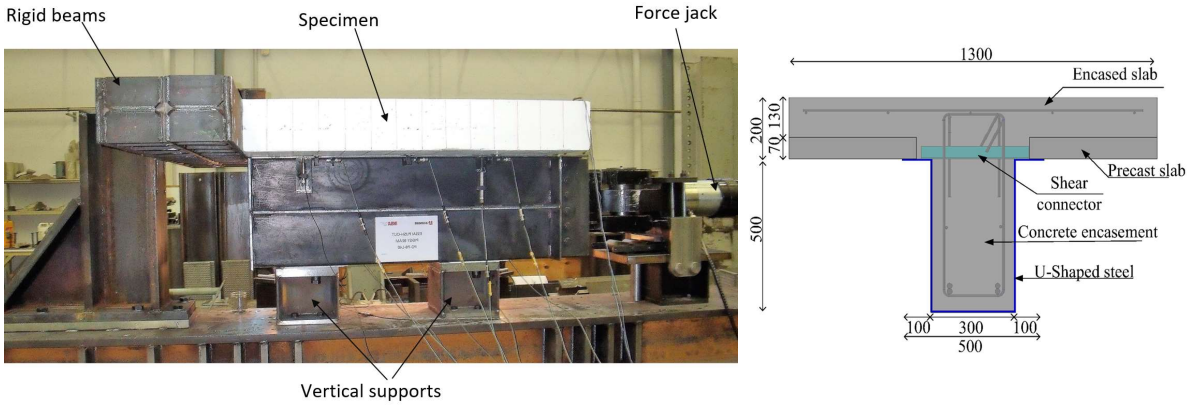

Figure 2: Test setup and specimens in pushout tests [7].

The failure mode of the specimens from the tests were the following. The failure of PO-L40 was governed by the connector fracture that was associated with the plastic deformation of the connector (see Figure 3a). A similar failure mode to PO-L40 was observed in the other three specimens PO-L50 (a,b,c) (see. Figure 3b).

(a). L40×40×4 (b). L50×50×5

Figure 3: Fracture of the shear connector [7].

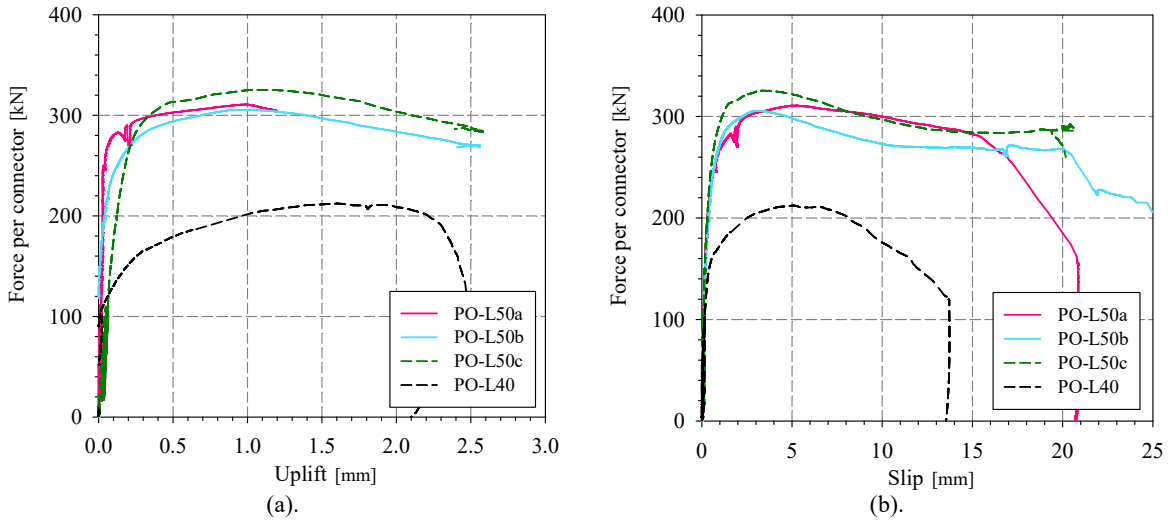

Figure 4: Load-mean slip/Load-mean uplift curves [7].

Figure 4 shows the relation between the push-out load and the mean slip as well as the mean uplift between the concrete and the steel beams. As observed in PO-L40 and PO-L50 (a, b, c), the L-shaped shear connectors were ductile and have a sufficient capacity in resisting the vertical separation between the concrete and steel components, which meets the requirement in the design codes for partial shear connection design [14].

A complete 3D finite element model was also developed and validated against the experimental results. The FE model was then used to perform a parametric study by evaluating the effect of parameters such as the concrete strength f_c, the cross-section of the L-shaped connector, the welded length of the shear connector to the upper flanges of the profile (L_w), as well as the thickness of concrete slab (H_c). Based on the results obtained from the parametric study, the equation for predicting the shear capacity of one L-shaped shear connector was proposed as following:

$$P_u = 2(A_{s1} + A_{s2})\frac{f_u}{\sqrt{3}} + 2K_c A_c f_c \quad (1)$$

where f_u is the ultimate strength of the connector; A_{s1}, A_{s2} and A_c are defined in Figure 5; and K_c is the calibration factor on concrete strength due to local pressure effect, defined from a regression analysis of the parametric study by the following expression:

$$K_c = 19 - 38.1\frac{H_a}{H_c} \quad (2)$$

in which, H_a and H_c are the cross-section height of the L-shaped connector and the thickness of the concrete slab, respectively.

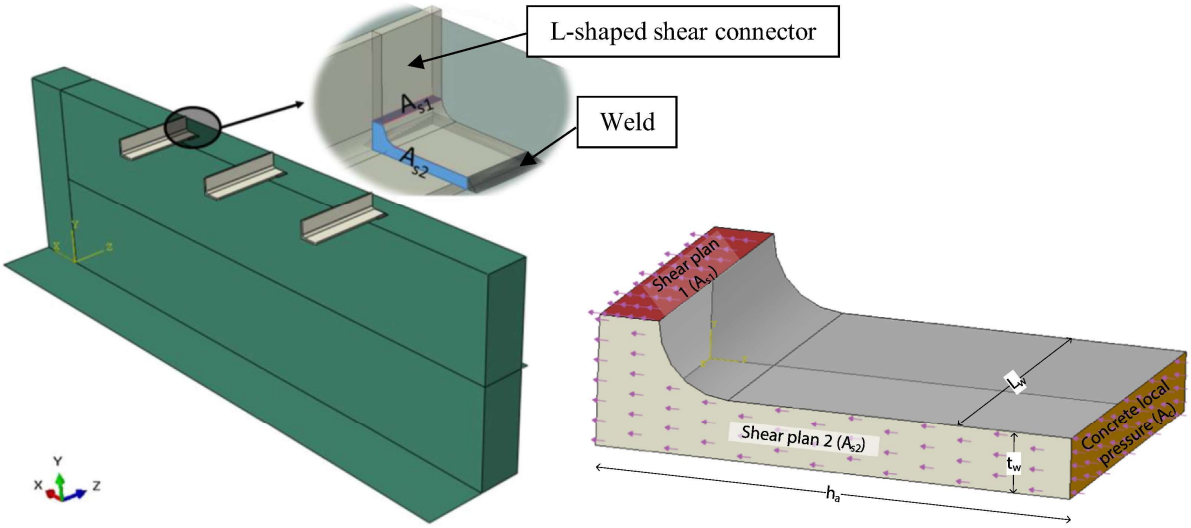

Figure 5: Shear sections and concrete pressure zones [7].

3. Experimental program

The present experimental program consists of bending tests on three full-scale specimens under positive bending moment. The main parameter for the investigation is the degree of shear connection. The first specimen, denoted by BM-1, was tested under a six-point bending configuration (see Figure 6a). The test on the second specimen was initially performed using the same configuration as BM-1; however, due to the limited capacity of the force jack, the maximum load was not reached. The specimen was then tested again but under a four-point bending configuration (Figure 6b). The second specimen is hereby denoted by BM-2(I) for the first phase of loading and BM-2(II) for the second phase. The last specimen, denoted by BM-3, was directly loaded with the four-point bending test.

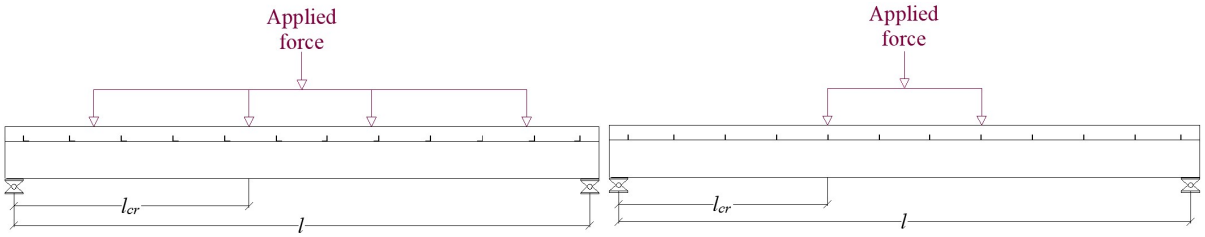

(a). Six-point configuration.

(b). Four-point configuration.

Figure 6: Bending test configurations used.

3.1 Test specimens

The specimens of the USCB, as illustrated in Figure 8, were composed of a U-shaped steel profile, concrete pre-cast panels, a reinforced concrete beam encased in the U-shaped steel profile, and L-shaped shear connectors. The dimensions of the specimens were chosen to conform to the design of the USCB in the AVRIL project. The information on the project and the design can be found in [16]. The U-shaped steel profile was made of cold formed steel with a constant thickness of 6 mm and a height of 500 mm. The bottom flange was 300 mm wide, and top flanges were 100 mm wide. The concrete slab was 200 mm high, and the total height of the USCB specimens is thus 700 mm. The concrete slab was also reinforced with the rebar mesh ST35, made of HA7 rebars with a spacing of 10 cm by 30 cm. In addition, the steel reinforcement of the concrete beam consisted of 4 HA16 rebars at the bottom, and 2 HA12 at the top, with a cover of 40 mm. The spacing of the HA8 stirrup, the dimension of the specimen, and the type and spacing of L-shaped shear connectors were different for each specimen. These details are provided in Table 1. The L-shaped shear connectors were welded to the upper flange of the U-shaped profile with the welding length of $L_{w1} = 40$ mm and $L_{w2} = 40$ mm for specimen BM-1 and $L_{w1} = 40$ mm and $L_{w2} = 50$ mm for specimens BM-2 and BM-3 (see Figure 7). The weld throat was 3 mm for the three specimens.

Table 1: Different details of each specimen.

Specimen	Dimensions		Stirrup	L-shaped connector			
	Width b [mm]	Length l [mm]		Type	Quantity	Length [mm]	Spacing [mm]
BM-1	2500	10610	HA8@430mm	40x40x4mm	38	380	260
BM-2(I)	1500	7790	HA8@350mm	50x50x5mm	12	380	700
BM-2(II)							
BM-3	1500	7790	HA8@220mm	50x50x5mm	18	380	430

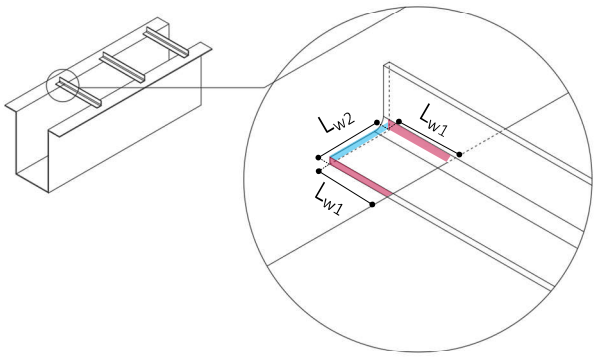

Figure 7: Detail of test specimens.

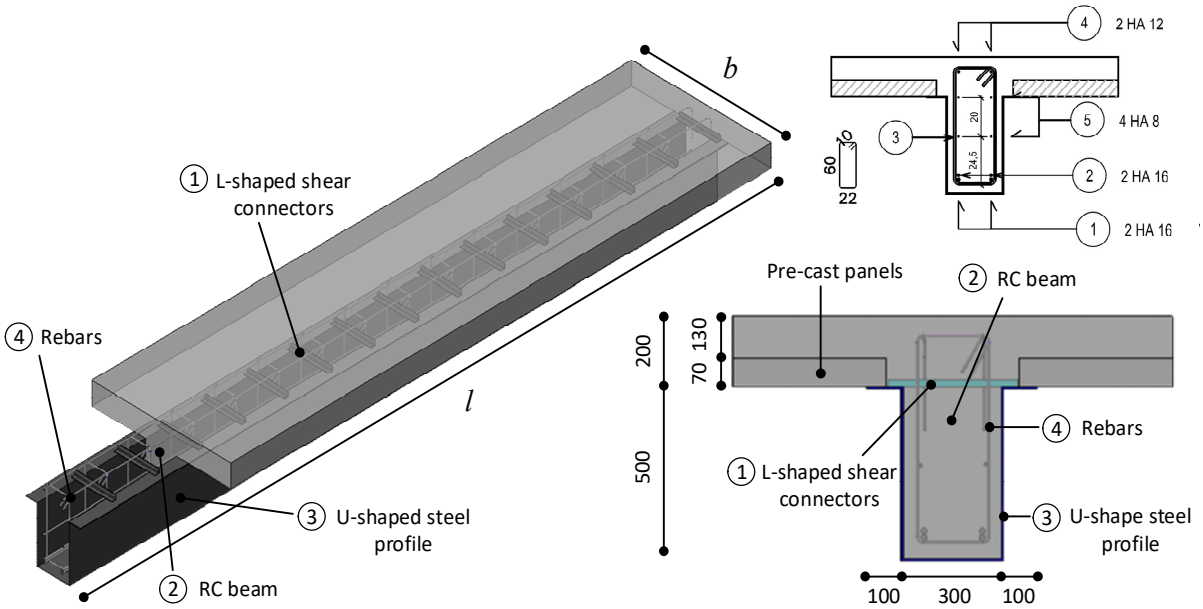

Figure 8: Detail of test specimens.

3.2 Material properties

The concrete has a strength class of C25/30 for the encased RC beam and C35/40 for the pre-cast panels. The concrete characteristics on the day of bending tests were determined on three cylinders samples with dimensions of 11×22 cm using cylinder concrete tests following the norm NF EN12390-3 [17]. The results of these tests are reported in Table 2, where f_{cm} and $\sigma_{f_{cm}}$ are the mean resistance of the concrete and its standard deviation. The steel grades of U-shaped steel beam, L-shaped steel profile and steel rebars are S355, S235 and B500B respectively. For each steel material, a tensile test was carried out following the norm NF EN ISO 6892-1 [18]. The results of these tests are reported in Table 3, in which f_y and f_u are the elastic and ultimate limits, respectively.

Table 2: Properties of the concrete.

Specimen	RC beam				Pre-cast panel			
	At 28 days		On the test day		At 28 days		On the test day	
	f_{cm} [MPa]	$\sigma_{f_{cm}}$ [MPa]	f_{cm} [MPa]	$\sigma_{f_{cm}}$ [MPa]	f_{cm} [MPa]	$\sigma_{f_{cm}}$ [MPa]	f_{cm} [MPa]	$\sigma_{f_{cm}}$ [MPa]
BM-1	26.03	0.17	27.41	1.53	48.36	1.64	48.89	0.99
BM-2(I)	26.66	0.19	26.66	0.19	-	-	53.53	0.75
BM-2(II)			29.99	0.23	-	-	-	-
BM-3	24.65	0.81	29.95	2.56	-	-	59.01	0.73

Table 3: Properties of the steel elements.

Specimen	U-shaped profile		L-shaped connector		Steel rebar	
	f_y[MPa]	f_u[MPa]	f_y[MPa]	f_u[MPa]	f_y[MPa]	f_u[MPa]
BM-1	412	481	345	471	-	-
BM-2(I)	412	481	343	467	557	627
BM-2(II)	412	481				
BM-3	430	540				

3.3 Test setup

The test setup was composed of a hydraulic force jack with a capacity of 1500 kN, a system of spreader beams, guiding columns, a specimen of the USCB, and a supporting system, as illustrated in Figure 9. In the test setup, the specimen of the USCB was simply supported on two supports. For one of the supports (see detail of support 1 in Figure 9), the rotation and the horizontal displacement were released with a hinge mechanism and with the use of the PTFE layers, respectively. For the other support (see detail of support 2 in Figure 9), the rotation was released, while the horizontal displacement was blocked at the upper flanges of the U-shaped steel profile (at the level of the elastic neutral axis of the composite cross-section). As already explained, the system of spreader beams had two configurations depending on the configuration of the bending tests (see Figure 10). The transversal displacement of the specimen was constantly controlled using the four guiding columns.

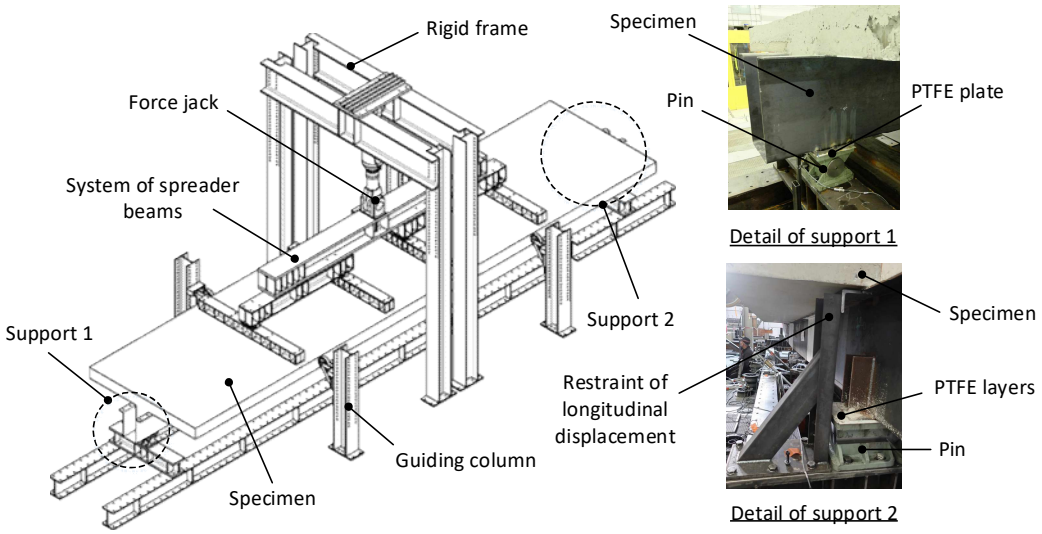

Figure 9: Test setup.

(a). Six-point bending test (b). Four-point bending test

Figure 10: Photos of test setups.

The degree of shear connection can be defined as the ratio of the total shear capacity of the shear connectors to the yield capacity of the steel beam:

$$\eta = \frac{nP_u}{A_s f_{y,U}} \tag{3}$$

where P_u is the ultimate resistance of one L-shaped shear connector, as being recalled in Section 2; A_s is the area section of the U-shaped steel profile; $f_{y,U}$ is the yield limit of the U-shaped steel profile; n is the number of shear connectors placed in the USCB on the critical length l_{cr}. The critical length is defined by a distance between zero and maximum bending moment points (see Figure 6 and Figure 10). The values of the degree of shear connection and of the critical length are given in Table 4 for each test. Since two configurations were used in the second test, two values of the degree of shear connection are defined.

Table 4: Degree of shear connection of the bending tests.

Specimen	Total Span l [mm]	x_1 [mm]	x_2 [mm]	Critical length l_{cr} [mm]	Degree of connection η
BM-1	10610	2460	2100	4560	1.14
BM-2(I)	7790	1060	2100	3160	0.5
BM-2(II)		2845	-	2845	0.41
BM-3		2845	-	2845	0.55

3.4 Loading procedure and instrumentation

The specimens were tested by applying a vertical load monotonically through the force jack with the system of spreader beams. For tests BM-1 and BM-2, the loading was split into three phases. In the first phase, two cycles of loading between zero and an estimated value of the load at serviceability limit state loading were applied. In the second phase, two more cycles of loading between zero and an estimated value of ultimate limit state loading were carried out. In the final phase, the loading was reapplied up to the failure of the specimen. For the test BM-3, the specimen was subjected to 25 cycles of loading between 5 kN and an estimated value of serviceability limit state loading, and 2 cycles of loading between 5 kN and an estimated value of ultimate limit state loading before loading incrementally up to failure.

To measure the deflection of the USCB, five LVDT sensors and one laser sensor (see Figure 11a) were installed along the length of the specimen. The laser sensor was placed at mid-span of the beam. The distribution of the slips between the steel and the concrete along the specimen was obtained by 8 horizontal LVDT sensors in the test BM-1 and by 16 horizontal sensors in tests BM-2 and BM-3. The sensors were fixed to the top flanges of the U-shaped profile, whereas the base was fixed onto the concrete slab, as illustrated in Figure 11b.

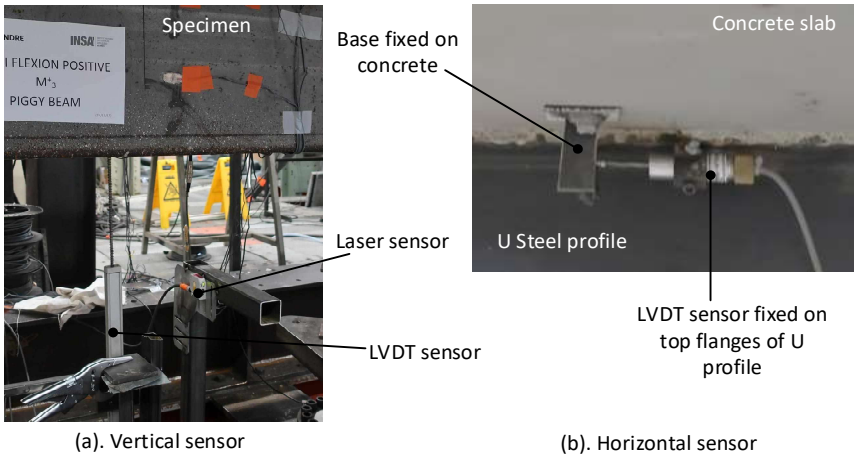

Figure 11: Vertical sensors and horizontal sensors.

Furthermore, the distribution of the deformations on the composite cross-section at midspan was determined by 19 strain gauges. 7 strain gauges were placed on the concrete, another 6 strain gauges were located on the U-shaped steel profile, and the other 6 were positioned on the rebars (see Figure 12).

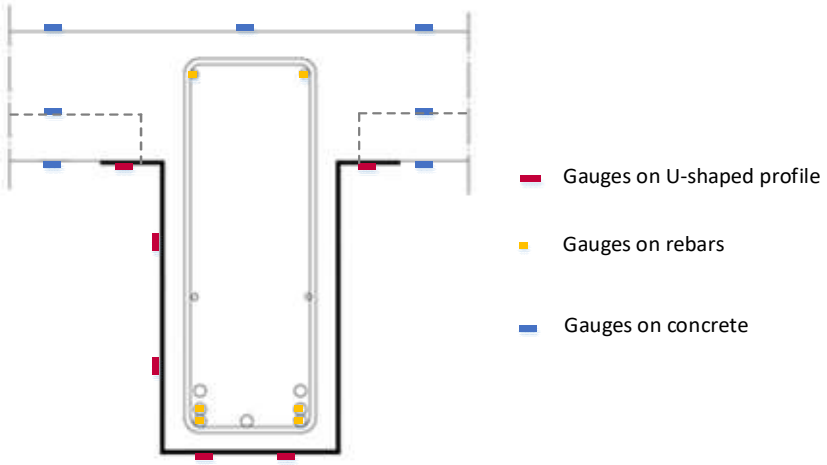

Figure 12: Strain gauges on the composite cross-section.

In addition to the analogue measurements, high-resolution photo cameras were also installed for a Digital Image Correlation analysis (DIC) on the zones indicated in Figure 13. In the side zones, the U-shaped steel profile was drilled with 10 circular openings of 20 mm in diameter, and small marks were glued on the concrete surface inside the opening and on the U-shaped profile next to it. A series of photos of these marks were captured during the course of the test at each increment of loading. After the tests, the photos were processed in order to obtain the

relative displacement of these marks, i.e. the slips between the steel and the concrete, using GOM Correlate Professional 2016 [19].

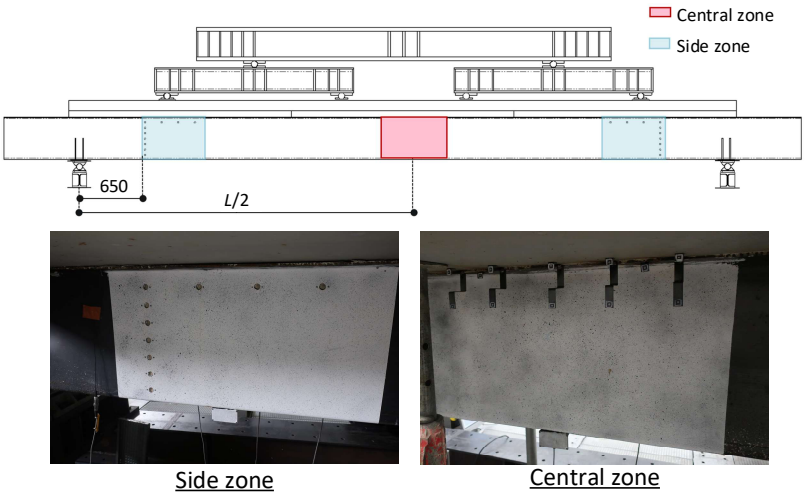

Figure 13: Zones of DIC measurement.

3.5 *Test results*

3.5.1 Moment-deflection responses and modes of failure

Figure 14 shows the moment-deflection curve at the mid-span of the specimen for the three tests. For test BM-1, a large value of the mid-span deflection superior than one fiftieth of the total span was obtained, showing the high ductility of the USCB in the case of full shear connection. In this test, a complete failure of the specimen was not however attained as the test was stopped when the verticality of the axis of the force jack was no longer ensured due to the nonlinear effects caused by the large deflections of the specimen. Figure 15 shows the deformed configuration of specimen BM-1 after the test.

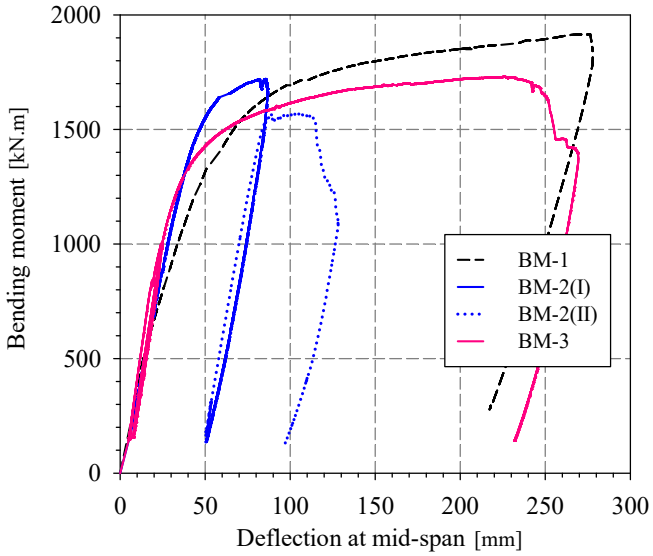

Figure 14: Moment-deflection curves.

Figure 15: Photo of the specimen BM-1 after the test.

In the test BM-2, it can be seen from the figure that the maximum value of the moment in the second phase of loading was lower than that in the first phase. The behavior of the test BM-2 was a lot less ductile than that of the test BM-3.

The failure mode of the two specimens (BM-2 and BM-3, cases with partial shear connection) was governed by the plastic buckling of the upper flanges of the U-shaped steel profile at the location of the shear connectors, as being shown in Figure 16 and Figure 17a. This plastic buckling was provoked by localized shear forces in combination with the rotation of the beam induced by the flexural load, which could be observed more prominently at the locations of larger bending moment. This plastic buckling was accompanied by the transverse concrete cracks at the location of the connectors (see Figure 17b).

Figure 16: Plastic buckling of the upper flanges of the U-shaped steel profile at locations of shear connectors.

(a). Plastic buckling. (b). Concrete cracks.

Figure 17: (a). Plastic buckling of the upper flange. (b). Concrete cracks at the location of shear connectors.

3.5.2 Steel-concrete slip behaviour

A. Slip distribution along the USCB length

Deduced from the horizontal sensors, the slips between the steel and the concrete beams at the top flange of the U-shaped profile along the beam axis are illustrated in Figure 18 for tests BM-1. The maximum bending moment M_u obtained in this test is 1915 kN.m. It can be seen from the figure that the maximum slip was around 2 mm, which is smaller than the ultimate slip (around 3 to 5 mm) of L-shaped shear connectors type L50 obtained from the pushout tests.

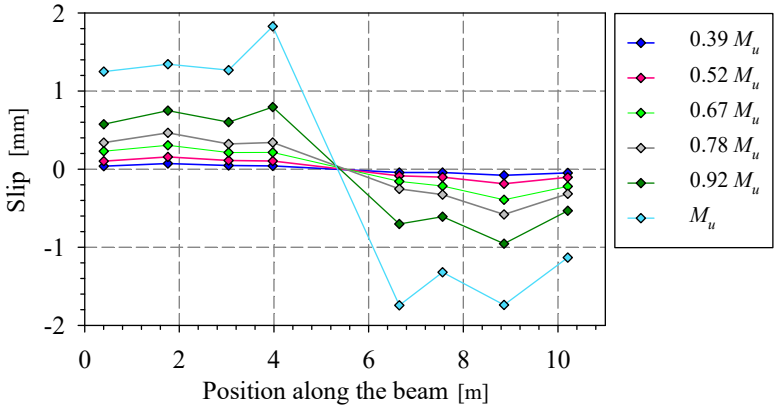

Figure 18: Distribution of slips along the beam axis in test BM-1.

Figure 19 and Figure 20 show the slip distribution along the beam axis for tests BM-2 and BM-3 at different load levels, respectively. It should be noted that the negative sign in the legends represent the descendent part of the bending moment-rotation curves after the peak. The maximum bending moments M_u obtained in tests BM-2(I), BM-2(II) and BM-3 are 1709 kN.m, 1600 kN.m and 1720 kN.m, respectively. The distribution of the slips in the test BM-2(II) became noticeably asymmetric after the moment reached 097M_u. From the figures, the maximum slips for test BM-2 and BM-3 exceeded the value of 15 mm, being quite larger than the ultimate slip (around 3 to 5 mm) of L-shaped connector type L50 obtained from pushout tests.

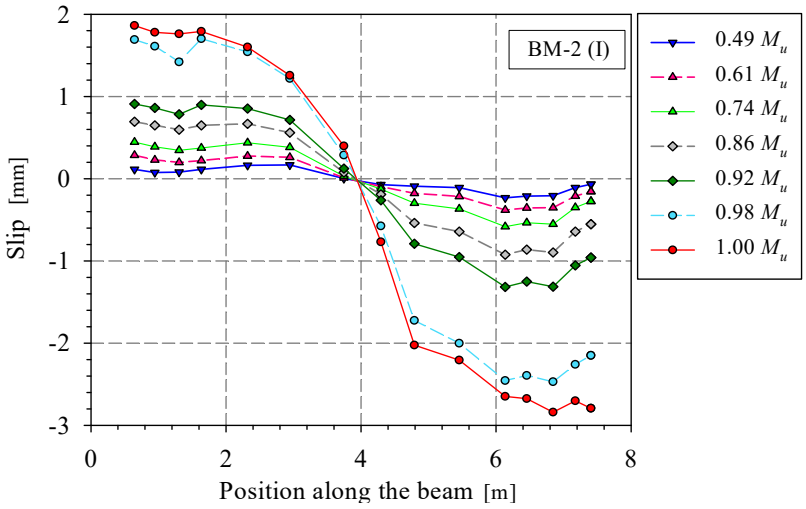

(a). Test BM-2(I).

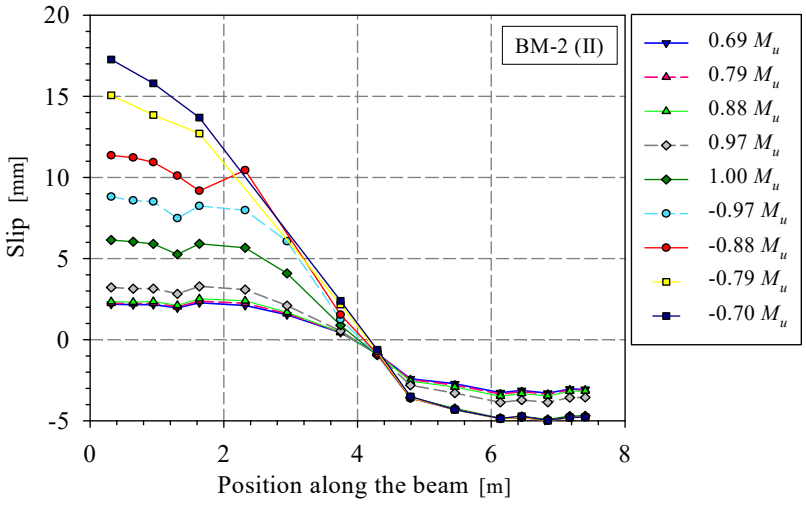

(b). Test BM-2(II).

Figure 19: Distribution of slips along the beam axis in tests BM-2.

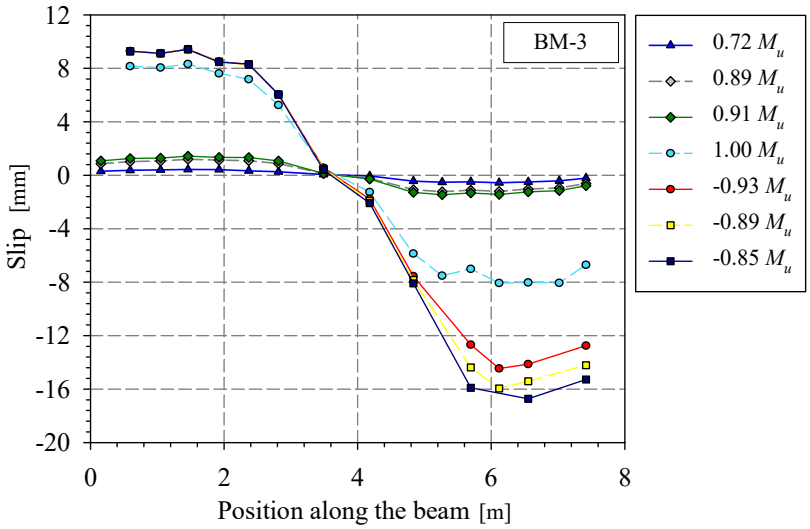

285

Figure 20: Distribution of slips along the beam axis in test BM-3.

B. Slip distribution along the cross-section depth of the USCB

The DIC analysis of the side zone (see Figure 13) allowed to determine the slip distribution between the steel and the concrete on the cross-section of the USCB. The numbering of the points where slips were measured is described in Figure 21. The evolution of the slips on the height of the cross-section is illustrated in Figure 22 for tests BM-2(II) and BM-3. It can be seen from the figure that the slips were almost constant on the height of the cross-section of the U-shaped steel profile for the tests with partial shear connection. This confirms that curvatures of the steel and of the concrete are nearly equal.

Figure 21: Numbering of points for measured slips.

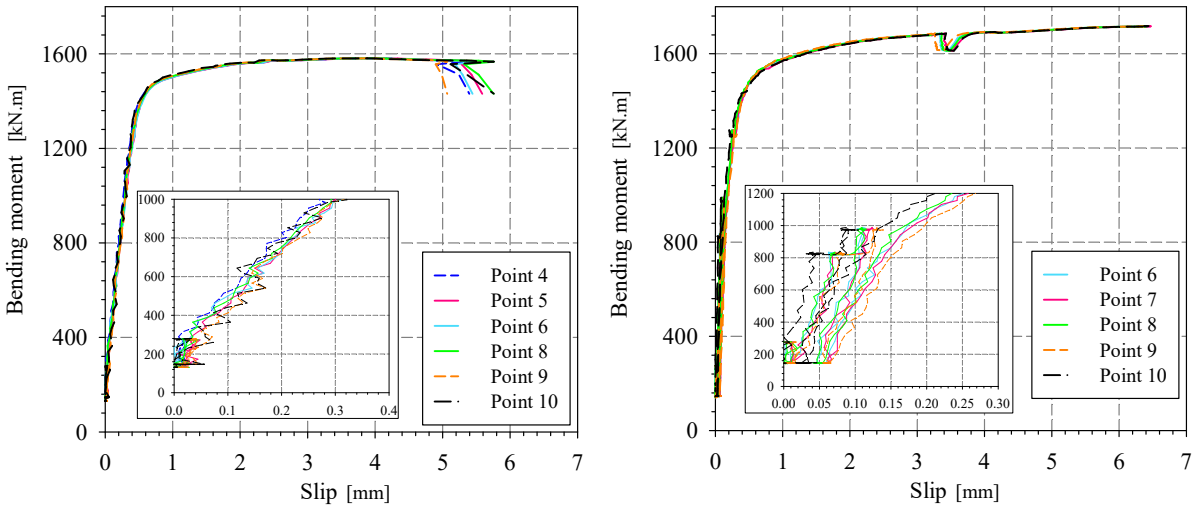

(a). Test BM-2(II). (b). Test BM-3.

Figure 22: Evolution of slips along the height of the cross-section in function of the bending moment.

C. Strain distribution over the cross-section depth of the USCB

In order to measure the distribution of the strains along the cross-section depth of the USCB, a number of strain gauges were installed on the cross-section (steel U-shaped profile, steel reinforcement and the concrete) as shown in Figure 12. The strain distribution for test BM-1 is described in Figure 23. In this test, the results from the strain gauges on the top surface of the precast concrete, on the steel rebars, and on the top flange of the U-shaped profile were not available. However, the strain distribution for this test in the case of full shear connection seems to be almost linear and continuous from the steel to the concrete cross-section. This result confirms the hypothesis of full shear connection with insignificant effects of the slips between the two cross-sections.

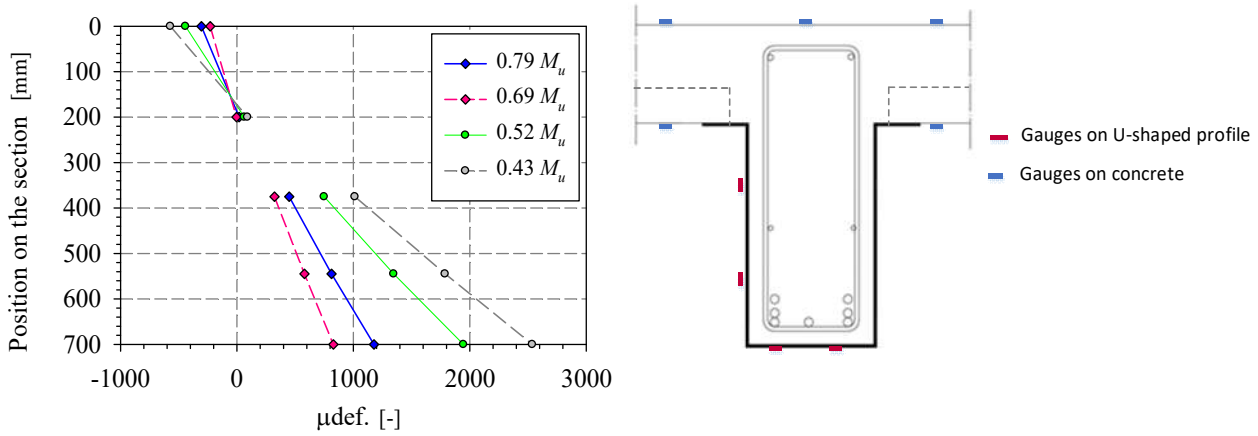

Figure 23: Strain distribution on the cross-section of the USCB for test BM-1.

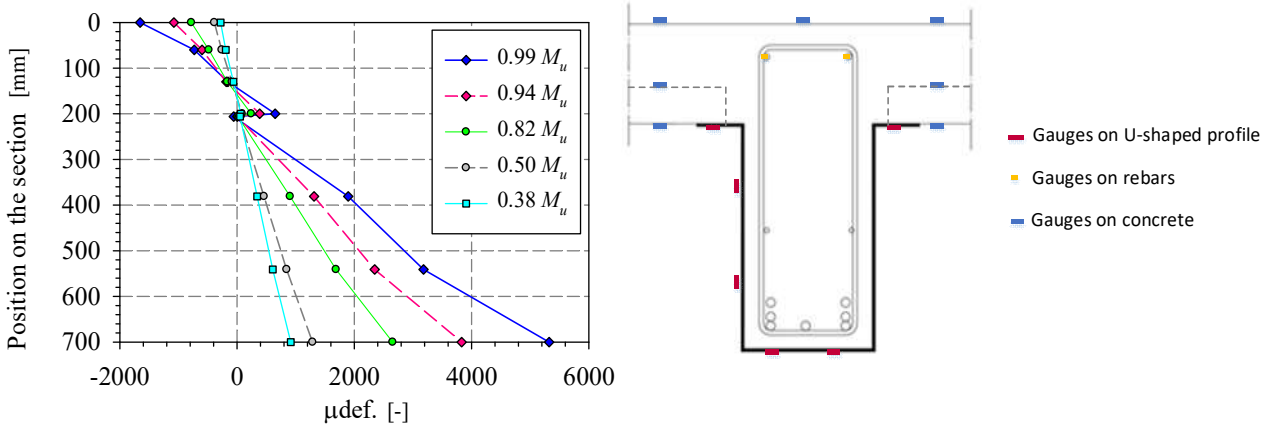

Figure 24: Strain distribution on the cross-section of the USCB for test BM-2(I).

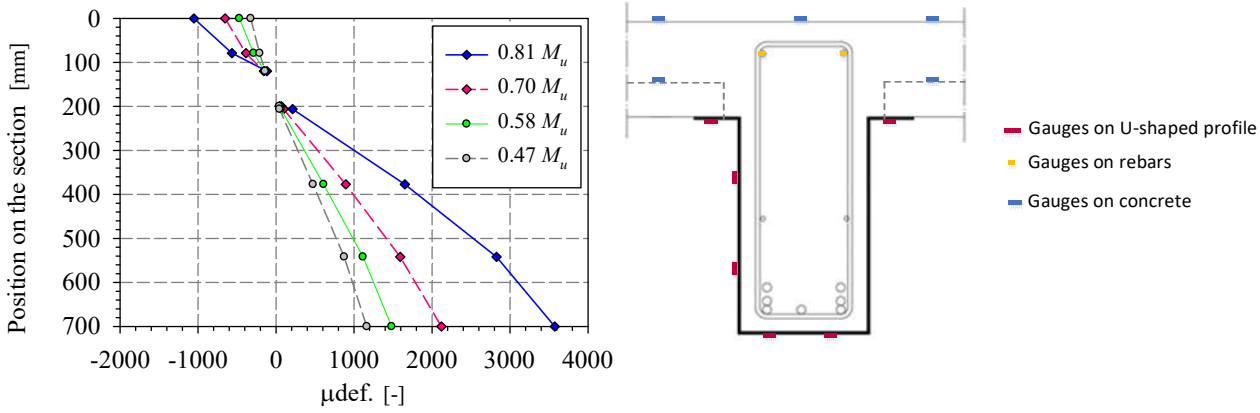

Figure 25: Strain distribution on the cross-section of the USCB for test BM-3.

Figure 24 and Figure 25 illustrate the strain distribution over the cross-section of the USCB for test BM-2(I) and BM-3, respectively. The discontinuity between the strains in the cross-section of the concrete slab and those in the U-shaped steel profile caused by the partial interaction is easily visible for the case of test BM-2(I). It is less intuitive for test BM-3, as the results from the strain gauges on the bottom surfaces of the concrete panels were not available.

4. Design approach for the USCB in partial shear connection

The slips occurring at the steel-concrete interface of the USCB due to the partial shear connection provided by the mechanical shear connectors can have substantial effects on the flexural stiffness and the bearing capacity of the composite beams. In this section, the existing design approaches in the current norms taking into account the partial shear connection are investigated with regard to the new configuration of the USCB. The results are then validated against the experimental results presented in Section 3.

4.1.1 Ultimate flexural bearing capacity

The flexural bearing capacity of the USCB can be computed using the plastic analysis method and taking into account the effect of the partial shear connection. Two approaches are investigated in this section. The first approach was initially proposed by Chen et al [4] for a new type of checkered steel-encased concrete composite beam. The second approach is the simplified method provided by Eurocode 4 [14] with a linear assumption based on the bearing capacity with full shear connection and without shear connection.

A. Full plastic analysis approach

The approach presented herein is based on the method proposed by Chen et al [4], adjusted to apply to the configuration of the USCB. It includes the relative slips between the concrete and the steel. The slips are assumed constant over the depth of the cross-section of the U-shaped profile, as can be seen in Figure 26. These slips give rise to two different positions of the plastic neutral axis (PNA) of the concrete (x) and of the steel (y). This generates three different cases for determining the bearing capacity :

- Case 1 occurs when the PNA of the concrete is found in the concrete slab and the PNA of the steel is in the web of the U-shaped profile (see Figure 27).
- Case 2 happens when the PNA of the concrete is in the concrete slab and the PNA of the steel is in the top flange of the U-shaped profile (see Figure 27).
- Case 3 comes about when the PNA of the concrete is in the U-shaped profile and the PNA of the steel is in the web of the U-shaped profile (see Figure 28). The case in which the PNA of the concrete is in the U-shaped profile and the PNA of the steel is in the top flange of the U-shaped profile is rare and not considered for the sake of simplicity.

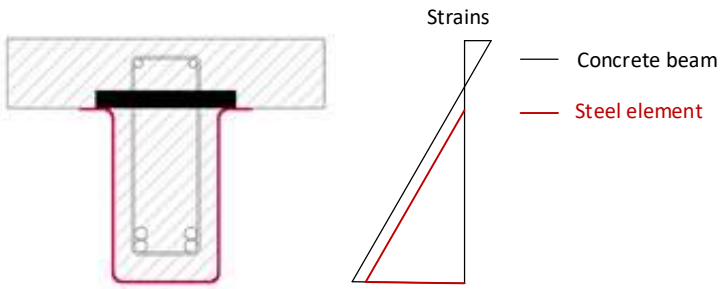

Figure 26: Strain on the cross-section of the USCB.

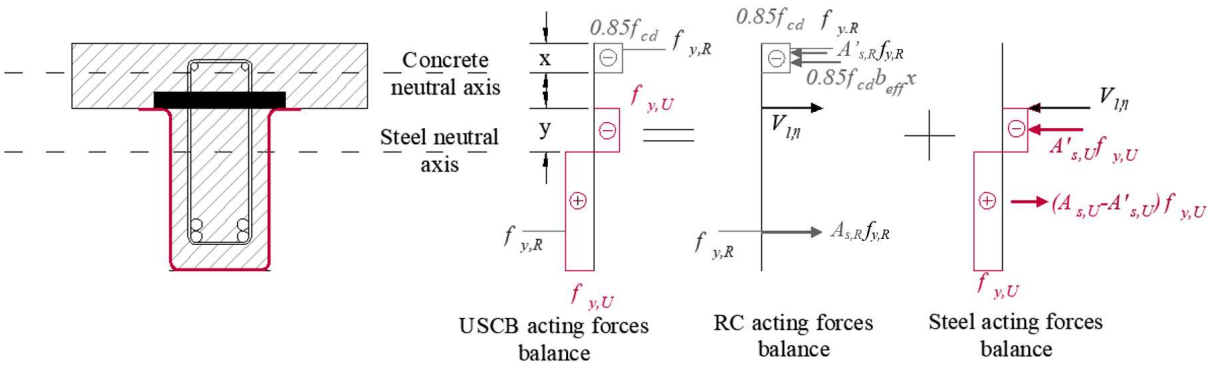

Figure 27: Model for computing the ultimate bearing capacity in Cases 1 and 2

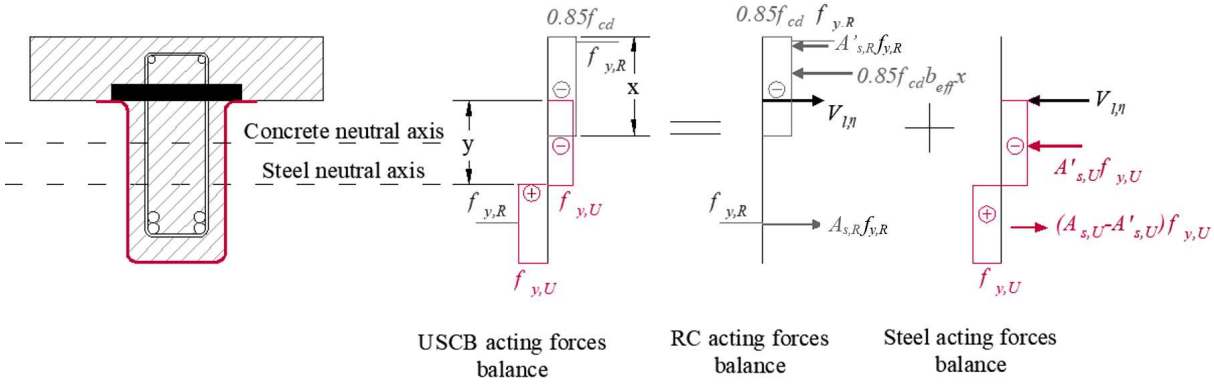

Figure 28: Model for computing the ultimate bearing capacity in Case 3.

The plastic equilibrium in the composite cross-section relies largely on the degree of shear connection η. The longitudinal shear force in the case of partial connection can be defined in relation to the degree of shear connection as:

$$V_{l,\eta} = \eta V_{l,1} \tag{4}$$

where $V_{l,1}$ is the longitudinal shear force in the case of full shear connection, defined by:

$$V_{l,1} = \begin{cases} A_{s,U} f_{y,U} & \text{if} \quad z < H_c \\ (A_{s,U} - 2A'_{s,U}) f_{y,U} & \text{if} \quad z \geq H_c \end{cases} \tag{5}$$

In which $A'_{s,U}$ is the cross-section area of the U-shaped profile for the compressive part. z is the neutral axis of the composite section in full connection.

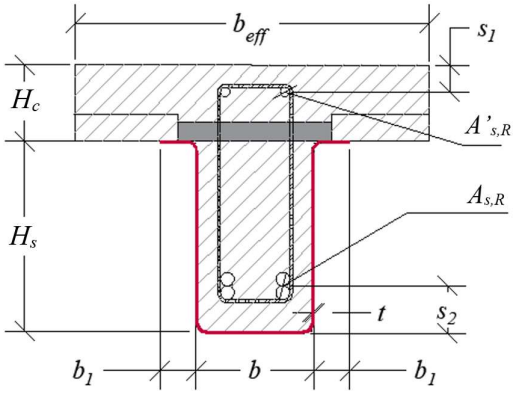

Figure 29: Parameters of the geometry of the cross-section.

The equilibrium on the composite cross-section can be decomposed into the equilibrium in the concrete cross-section and that in the steel cross-section with the load transfer mechanism by the shear connectors. The equilibrium equations of the concrete cross-section can be used to compute the position of the neutral axis of the concrete section. Two cases exist :

- $x < H_c$ (see Figure 27):

$$b_{\text{eff}} x 0.85 f_{cd} + A'_{s,R} f_{y,R} = A_{s,R} f_{y,R} + V_{l,\eta} \tag{6}$$

which gives

$$x = \frac{-A'_{s,R} f_{y,R} + V_{l,\eta} + A_{s,R} f_{y,R}}{b_{\text{eff}} 0.85 f_{cd}} \tag{7}$$

- $x \geq H_c$ (see Figure 28):

$$(b_{\text{eff}} - b) H_c 0.85 f_{cd} + 0.85 f_{cd} (b - 2t) x + A'_{s,R} f_{y,R} = A_{s,R} f_{y,R} + V_{l,\eta} \tag{8}$$

which gives

$$x = \frac{-(b_{\text{eff}} - b) H_c 0.85 f_{cd} - A'_{s,R} f_{y,R} + V_{l,\eta} + A_{s,R} f_{y,R}}{b_{\text{eff}} 0.85 f_{cd}} \tag{9}$$

where b_{eff} is the effective width of the concrete block (see Figure 29), determined according to Eurocode 4 [14]. H_c and b are the height of the concrete slab and the width of the bottom flange of the U-shaped steel profile, respectively. f_{cd} is the design value of the compressive strength of the concrete and Chen et al [4] limit the stress in concrete to $0.85 f_{cd}$. $f_{y,R}$ is the design value of the yield limit of the steel rebars. $A'_{s,R}$ and $A_{s,R}$ are the top and bottom cross-section areas of the rebars, respectively.

The equilibrium equation on the steel cross-section can be written as:

$$(A_{s,U} - A'_{s,U}) f_{y,U} = A'_{s,U} f_{y,U} + V_{l,\eta} \tag{10}$$

where $A'_{s,U}$ is the cross-section area of the U-shaped profile for the compressive part, which can be deduced from Eq. (10) as:

$$A'_{s,U} = \frac{A_{s,U} f_{y,U} - V_{l,\eta}}{2 f_{y,U}} \tag{11}$$

Subsequently, the position of the PNA of the steel element can be determined as following:

$$\begin{cases} y = \dfrac{A'_{s,U}}{2b_1} & \text{if } y < t \\ y = \dfrac{A'_{s,U} - 2b_1 t}{2t} & \text{if } y \geq t \end{cases} \tag{12}$$

where t and b_1 are the thickness of the U-shaped profile and the width of the top flange of the U-shaped steel profile, respectively (see Figure 29).

Finally, the ultimate bending resistance of the USCB in partial shear connection ($M_{pl,Rd,\eta}$) can be determined according to the cases as following:

- Case 1 ($y \geq t$ and $x < H_c$)

$$M_{pl,Rd,\eta} = A'_{s,R}f_{y,R}\left(\frac{x}{2} - s_1\right) - 2tb_1f_{y,U}\left(H_c + \frac{t}{2} - \frac{x}{2}\right) - 2tyf_{y,U}\left(\frac{y}{2} + H_c - \frac{x}{2}\right) + 2tf_{y,U}(H_s - y)\left(\frac{H_s + y}{2} + H_c - \frac{x}{2}\right) + (b - 2t)tf_{y,U}\left(H_s - \frac{t}{2} + H_c - \frac{x}{2}\right) + A_{s,R}f_{y,R}\left(H_s + H_c - \frac{x}{2} - s_2\right) \quad (13)$$

where H_s, s_1 and s_2 are defined in Figure 29.

– Case 2 ($y < t$ and $x < H_c$)

$$M_{pl,Rd,\eta} = A'_{s,R}f_{y,R}\left(\frac{x}{2} - s_1\right) - 2(b_1 + t)yf_{y,U} + 2(b_1 + t)f_{y,U}(t - y)\left(\frac{t + y}{2} + H_c - \frac{x}{2}\right) + 2tf_{y,U}(H_s - 2t)\left(\frac{H_s}{2} + H_c - \frac{x}{2}\right) + btf_{y,U}\left(H_s - \frac{t}{2} + H_c - \frac{x}{2}\right) + A_{s,R}f_{y,R}(H_s + H_c - \frac{x}{2} - s_2) \quad (14)$$

– Case 3 ($y \geq t$ and $x > H_c$)

$$M_{pl,Rd,\eta} = -A'_{s,R}f_{y,R} - 2tb_1f_{y,U}\left(H_c + \frac{t}{2}\right) - 2tyf_{y,U}\left(\frac{y}{2} + H_c\right) + 2tf_{y,U}(H_s - y)\left(\frac{H_s}{2} + \frac{y}{2} + H_c\right) + (b - 2t)tf_{y,U}\left(H_s + H_c - \frac{t}{2}\right) + A_{s,R}f_{y,R}(H_s + H_c - s_2) - \frac{0.85f_{cd}\left(b_{eff} - b + 2t\right)H_c^2}{2} - \frac{0.85f_{cd}(b - 2t)x^2}{2} \quad (15)$$

B. Simplified approach by Eurocode 4

The approach provided by Eurocode 4 [14] adopts the rigid plastic theory for determining the ultimate bearing capacity of the composite beam with full shear connection. In this case, the PNA of the composite cross-section is assumed to locate in the concrete slab. In the case of partial shear connection, Eurocode 4 [14] proposes a linear simplification as following:

$$M_{pl,Rd,\eta} = M_{pl,Rd,0} + \left(M_{pl,Rd,1} - M_{pl,Rd,0}\right)\eta \quad (16)$$

where $M_{pl,Rd,1}$ is the ultimate bearing capacity of the composite beam with full shear connection. $M_{pl,Rd,0}$ is the ultimate bearing capacity of the composite beam with zero shear connection. For conventional composite beams, i.e. I-profile steel composite beam, $M_{pl,Rd,0}$ can be taken equal to the plastic bending resistance of the steel beam. However, in the case of the USCB, the concrete contribution cannot be neglected. Consequently, $M_{pl,Rd,0}$ is the combination of the plastic bending resistance of the steel beam ($M_{pl,Rd,U}$) and the ultimate bending resistance of the concrete beam ($M_{pl,Rd,RC}$), which is defined as following:

$$M_{pl,Rd,0} = M_{pl,Rd,U} + M_{pl,Rd,RC} \quad (17)$$

The computation of $M_{pl,Rd,RC}$ and $M_{pl,Rd,U}$ can be done following the design formulations provided in Eurocode 2 [20] and in Eurocode 3 [21], respectively.

C. Comparison between the experiment and the design approaches

The experimental results are used to evaluate the two design approaches. By adopting the empiric approach proposed by Aribert and Alain [22] to the moment-rotation curves in Figure 14, the ultimate bending capacities ($M_{pl,Rd,\eta}$) for test BM-1, BM-2(I), BM-2(II) and BM-3 are 1887 kN.m, 1709 kN.m, 1600 kN.m and 1578 kN.m, respectively. In order to be able to compare the results, the values of $M_{pl,Rd,\eta}$ are normalized with the ultimate bending capacities with full shear connection ($M_{pl,Rd,1}$) and presented in function of the degree of shear connection in Figure 30. As can be seen from this figure, the values obtained from the full plastic analysis approach agree well with the experimental results obtained from tests BM-1 and BM-3. However, some difference is obtained when compared with the tests BM-2(I) and BM-2(II). This might be due to the inaccurate calculation of the real degree of shear connection of the tests. In test BM-2, the actual degree of shear connection is indeed higher, as the friction between the steel and the concrete was not reduced by the so-called initial 25-cycle loading/unloading procedure prior to the monotonic loading to collapse, as having been done in test BM-3. In the case of test BM-1, this initial cycle loading procedure did not influence the resistance as full shear connection was achieved.

It can be concluded at this point that both design approaches presented here seem applicable for determining the ultimate bending capacity of the USCB; however, the full-plastic analysis approach gives more accurate results than the simplified approach provided in Eurocode 4 [14] when compared to the experimental results.

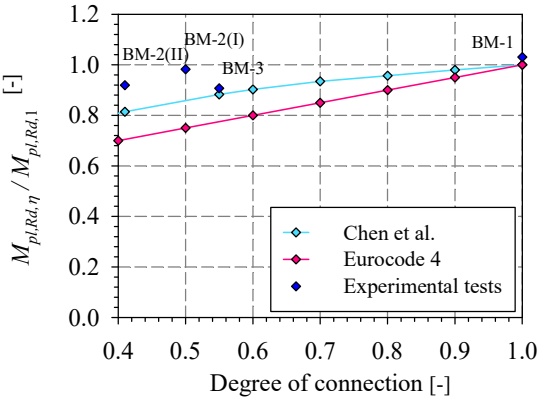

Figure 30: Normalized ultimate bending capacity of the USCB as a function of the degree of shear connection.

4.1.2 Flexural stiffness of the USCB

An accurate computation procedure of the deflection is needed in order to verify the requirements in serviceability limit states. For composite beams, noticeable differences exist between standards. It is indicated that the degree of shear connection can have an impact on the elastic flexural stiffness in some norms [23][24][25], whereas Eurocode 4 [14] neglects it when the degree of shear connection is superior to 0.5.

The British standard [23] provides the following expression for computing the deflection of the composite beams:

$$\delta_\eta = \delta_1 \left(1 + 0.5(1-\eta)\left(\frac{\delta_0}{\delta_1}\right)\right) \tag{18}$$

where δ_1 and δ_0 are the deflections of the USCB in the case of full shear connection and in the case of zero shear connection, respectively. Based on Eq. (18), Ban and Bradford [26] wrote the expression of the moment of inertia of the composite cross-section ($I_{\text{eff},\eta}$) in function of the degree of shear connection as following:

$$I_{\text{eff},\eta} = \frac{2I_0 I_1}{(1+\eta)I_0 + (1-\eta)I_1} \tag{19}$$

where I_1 and I_0 are the moments of inertia of cross-section of the composite beam in the case of full shear connection and in the case of zero shear connection, respectively. The American design standard AISC 360-05 [24] gives another expression for the moment of inertia as below:

$$I_{\text{eff},\eta} = (I_0 + \sqrt{\eta}(I_1 - I_0)) \tag{20}$$

Furthermore, the Australian standard AS 2327.1 [25] imposes another expression for computing the moment of inertia of composite beams, as described below:

$$I_{\text{eff},\eta} = I_0 + 0.6(1-\eta)(I_1 - I_0) \tag{21}$$

In order to compare the results obtained from the various expressions from the different standards with the experimental results, it is needed to determine the value of the bending moment at the SLS in the quasi-permanent combination ($M_{SLS,\eta}$), which is defined here as following:

$$M_{SLS,\eta} = kM_{pl,Rd,\eta} \tag{22}$$

where k is a reduction coefficient, being the ratio between the value from the load combination at serviceability limit state (quasi permanent) and the one at ultimate limit state. As indicated in Eurocode 0 [27], the load combinations for SLS-quasi permanent and for ULS are given as:

$$p_{SLS-quasi} = G + 0.3Q \tag{23}$$

$$p_{ULS} = 1.35G + 1.5Q \tag{24}$$

with G and Q, being the permanent and variable actions, respectively. In the case of the present study, a 60-40 distribution between the permanent and variable actions is assumed, giving the following relation:

$$\frac{G}{Q} = \frac{60}{40} \tag{25}$$

By inserting Eq. (25) into Eqs. (23) and (24), the coefficient k can be determined as

$$k = \frac{p_{SLS-quasi}}{p_{ULS}} = 0.51 \tag{26}$$

Consequently, the values of $M_{SLS,\eta}$ for test BM-1, BM-2(I) and BM-3 are 970 kN.m, 903 kN.m and 913 kN.m, respectively. The deflection corresponding to the value of $M_{SLS,\eta}$ in the experimental tests can then be deduced from the moment-deflection curves (see Figure 14).

Figure 31 illustrates the comparison of the normalized deflection curves obtained from the different standards with the results obtained from the experimental tests, corresponding to the value of $M_{SLS,\eta}$. It can be seen from the figure that the curves obtained from the Australian standard and from the American standard fit best to the experimental results. Table 5 provides margins of errors of the results estimated by different standards compared to the experimental results. Consequently, it can be concluded that the American and Australian standards are suitable for computing the flexural stiffness of the USCB with partial shear connection. The British standard seems to underestimate while the European standard appears to overestimate the flexural stiffness.

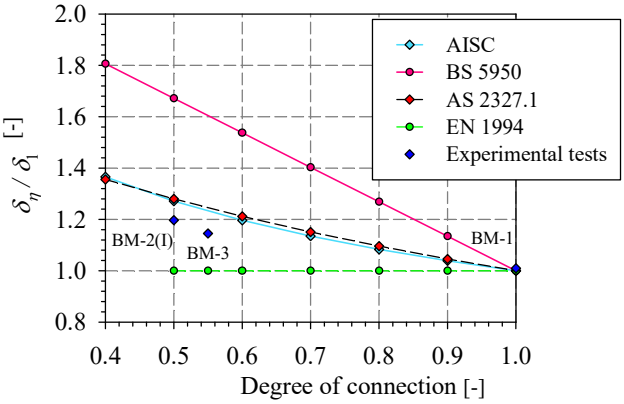

Figure 31: Normalized deflection curves in function of the degree of shear connection.

Table 5: Margins of errors of the results estimated by different standards compared to the experimental results.

Test	η	American standard	British standard	Australian standard	European standard
BM-1	1.14	0.01	0.01	0.01	0.01
BM-2(I)	0.5	0.06	0.4	0.07	0.2
BM-3	0.55	0.08	0.4	0.09	0.15

5. Numerical investigation

Nguyen [28] developed finite element formulations to determine the response of steel-concrete composite beams with discrete and continuous partial interactions, taking into account the material nonlinearity. However, the account for large displacements was not included. For the large-displacement analysis of steel-concrete composite beams, a good amount of research has been devoted to the development of beam models taking into account the interlayer slips [29]-[31] in the co-rotational framework. Battini et al [29] adopted the Bernoulli's assumption (plane sections remain plane) and the local formulation based on the exact solution of the governing equations for the composite beam with deformable shear connection. The use of the analytical local stiffness matrix

in their formulation permits to avoid the curvature locking that is usually encountered with low order polynomial finite elements, particularly for short elements with stiff shear connection. Keo et al [30] further extended the model for large displacement analysis of hybrid steel–concrete beam/column with several encased steel profiles. On the other hand, Hjiaj et al [31] took into account the transverse shear deformation of the layers of the composite beams by assuming that each layer of the composite beam behaved as a Timoshenko beam element. Assuming a continuously connected and partial interaction, a continuous relationship between the longitudinal shear flow and the corresponding slip at the interface between the layers was considered. The exact local stiffness derived from the closed-form solution of the governing equations of a two-layer beam was used to avoid the curvature and shear locking phenomena.

In this paper, in order to analyze the behavior of the USCB, the two-layer beam element formulation taking into account the interlayer slips with continuous connection is adopted. We adopt the governing equations of the local linear element described by Nguyen [28] and the kinematics in the co-rotational framework presented by Battini et al [29].

5.1 Local linear element

In this section, the field equations for a two-layered beam element with partial shear interaction are recalled. The concrete and the U-shaped profile are assumed to deform according to Bernoulli's assumption (plane sections remain plane). The interlayer connection is assumed to be continuously distributed.

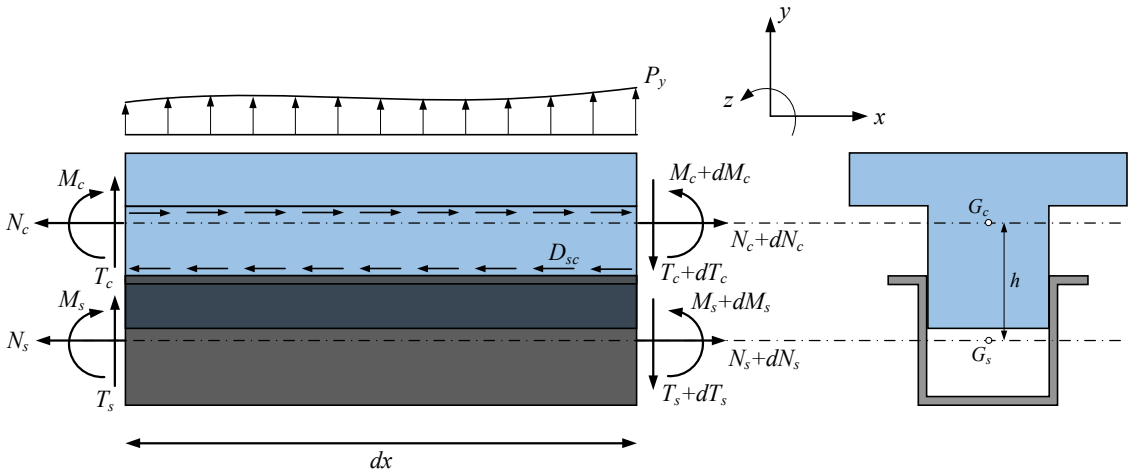

Figure 32: Free body diagram of a two-layer beam on an infinitesimal segment.

The equilibrium equations are derived by considering an infinitesimal beam segment at an arbitrary position x (see Figure 32) and are given as following:

$$\partial \boldsymbol{D} - \partial_{sc} D_{sc} - \boldsymbol{P}_e = 0 \tag{27}$$

where $\boldsymbol{D} = [N_s \quad N_c \quad M]^T$; $M = M_s + M_c$; $\boldsymbol{P}_e = [0 \quad 0 \quad p_y]^T$ and the operators ∂ and ∂_{sc} are defined by

$$\partial = \begin{bmatrix} \frac{d}{dx} & 0 & 0 \\ 0 & \frac{d}{dx} & 0 \\ 0 & 0 & -\frac{d^2}{dx^2} \end{bmatrix}; \; \partial_{sc} = \begin{bmatrix} 1 & -1 & h\frac{d}{dx} \end{bmatrix}$$

in which h is the distance between the elastic centroids of the layers cross-sections.

The U-shaped profile and the concrete are assumed to have the same transverse displacement, neglecting the uplift between the two members. Therefore, the rotation of the U-shaped and that of the concrete are the same, meaning that the slip is constant on the height of the cross-section. Under Bernoulli's assumption, the axial deformations (ε_s and ε_c) and the curvature κ are related to the beam displacements (see Figure 33) by :

$$\partial \boldsymbol{d} - \boldsymbol{e} = 0 \tag{28}$$

$$\partial_{sc} \boldsymbol{d} - g = 0 \tag{29}$$

where $\boldsymbol{d} = [u_s \quad u_c \quad v]^T$ is the displacement vector and $\boldsymbol{e} = [\varepsilon_s \quad \varepsilon_c \quad \kappa]^T$ is the deformation vector. The slip can also be computed by

$$g = u_c - u_s - h\theta \tag{30}$$

In order to avoid curvature locking in the two nodes beam elements, 10 degrees of freedom are considered as presented in Figure 34. Thus, an extra procedure is needed to obtain a tangent operator consistent with the co-rotational formulation, due to the intermediate nodes. The polynomial cubic function (Hermitiens) is used to approach the transversal displacement, whereas the linear function is adopted to approximate the axial displacements.

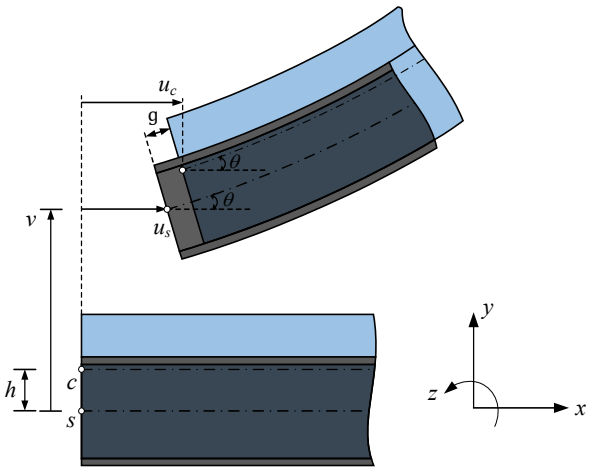

Figure 33: Kinematics of the composite beam.

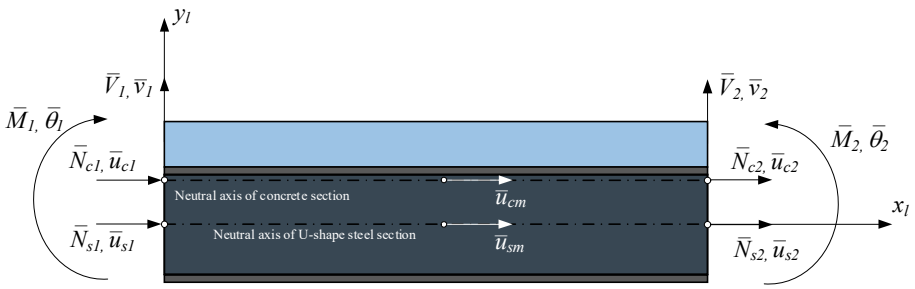

Figure 34: Local structural member.

5.2 Kinematics

The structural member consists of two sub-elements: a structural U-shaped steel profile (denoted by subscript "s") and a reinforced concrete beam (denoted by subscript "c"), as illustrated in Figure 35. The co-rotational framework is applied to the structural member. The origin of the co-rotational frame is taken at node s_1 located at the centroid of the cross-section of the U-shaped steel. The x_l-axis of the local coordinate system is defined by the line connecting node s_1 to node s_2.

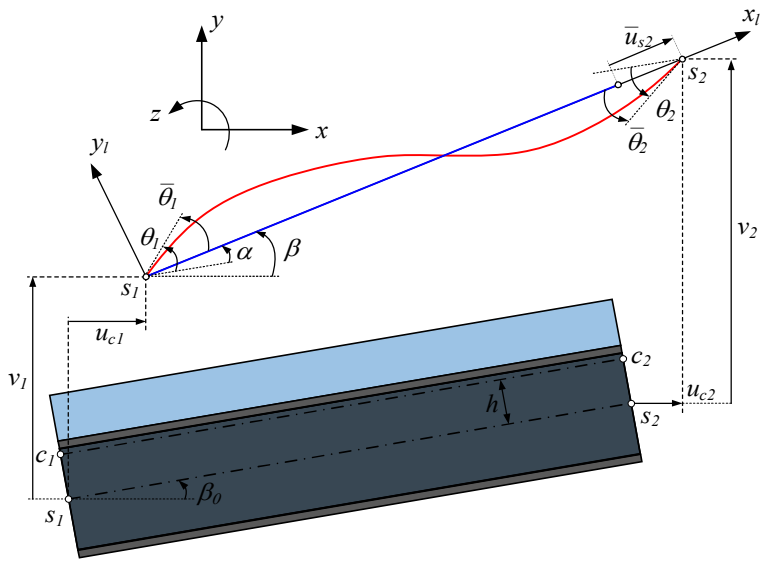

Figure 35: Co-rotational kinematic: displacements and rotations.

The y_l-axis is orthogonal to the x_l-axis so that the result is right hand-sided orthogonal coordinate system. The motion of the element from the original undeformed configuration to the actual deformed configuration can be separated into two parts. The first one, which corresponds to rigid motion of the local frame, is the translation of node s_1 and the rotation α of the x_l-axis (see Figure 35). The second one refers to the deformations in the co-rotating element frame.

The vectors of global and local displacements are respectively defined by:

$$\boldsymbol{P}_g = [u_{c1} \quad v_1 \quad \theta_1 \quad g_1 \quad u_{c2} \quad v_2 \quad \theta_2 \quad g_2]^{\mathrm{T}} \tag{31}$$

$$\boldsymbol{P}_l = [\bar{u}_{s1} \quad \bar{u}_{c1} \quad \bar{v}_1 \quad \bar{\theta}_1 \quad \bar{u}_{s2} \quad \bar{u}_{c2} \quad \bar{v}_2 \quad \bar{\theta}_2]^{\mathrm{T}} \tag{32}$$

Based on the definition of the co-rotating frame, the components of the local displacements $\boldsymbol{P}_l$ are determined as following:

$$\bar{u}_{c1} = 0 \tag{33}$$

$$\bar{v}_1 = 0 \tag{34}$$

$$\bar{v}_2 = 0 \tag{35}$$

$$\bar{u}_{c2} = l_n - l_0 \tag{36}$$

$$\bar{\theta}_1 = \theta_1 - \alpha \tag{37}$$

$$\bar{\theta}_2 = \theta_2 - \alpha \tag{38}$$

$$\bar{u}_{s1} = \bar{g}_1 - h_s\bar{\theta}_1 \tag{39}$$

$$\bar{u}_{s2} = \bar{g}_2 + \bar{u}_{c2} - h_s\bar{\theta}_2 \tag{40}$$

where the local slips are defined in function of the global slips (see Figure 36) by:

$$\bar{g}_1 = g_1 \cos\bar{\theta}_1 \tag{41}$$

$$\bar{g}_2 = g_2 \cos\bar{\theta}_2 \tag{42}$$

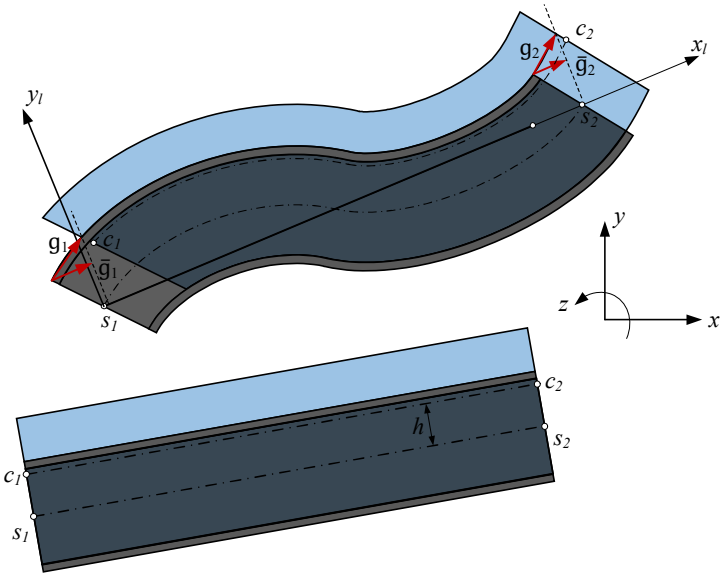

Figure 36: Local structural member.

5.3 Material models

An integration of the appropriate uniaxial constitutive model over each cross-section of the composite beam is needed to obtain the constitutive relationships of the section. A multi-fiber approach is adopted in order to integrate

the non-homogeneity of the concrete cross-section. The discretization of the cross-section is illustrated in Figure 37.

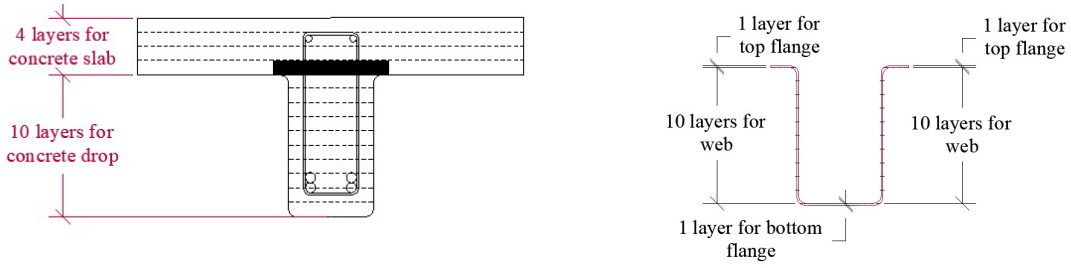

(a). Concrete section.

(b). Steel section.

Figure 37: Discretization of the cross-section.

The steel materials are modeled by an elastic-perfectly-plastic model, as illustrated in Figure 38a for U-shaped steel and Figure 38b for steel rebars. For the concrete material, the uniaxial constitutive relation is constructed from the stress-strain curve (see Figure 38c) provided by EN 1992-1-1 [20] and applied in the plasticity framework.

Regarding the behavior of the connector, we adopted a nonlinear force-slip relation as following:

$$P = P_u\left(1 - e^{-2\delta^{0.5}}\right) \tag{43}$$

where δ is the slip in mm and P_u is the resistance of the connector defined by Eq. (1). The expression of Eq. (43) is obtained from a calibration of the mean curve of the force-slip curves for test PO-L50a, PO-L50b and PO-L50c in Figure 4.

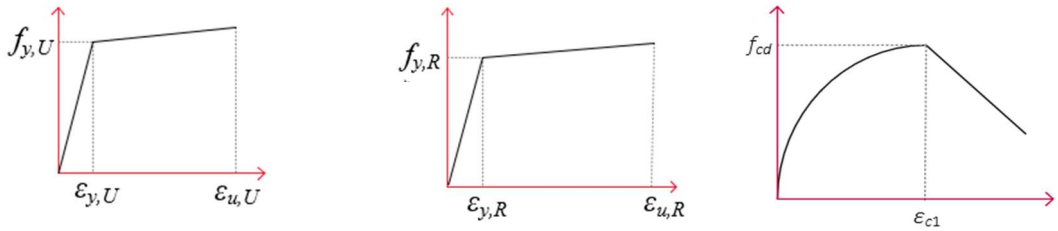

(a). U-steel element

(b). Rebars

(c). Concrete

Figure 38: Stress-strain curves for material modeling.

5.4 Validation of the numerical model

5.4.1 Validation against experimental results

In order to validate the numerical model, the actual material properties and the geometry of the USCB in the flexural tests (see section 3) were used in the numerical applications of the model. In the model, only a half of the beam length is considered while applying a symmetrical condition to one end of the beam to save the calculation time, with the loading and boundary conditions as illustrated in Figure 39 . The beam is discretized into 11 elements

along the length with an element size of approximately 50 cm for the case of test BM-1 or 8 elements with an element size of approximately 50 cm for the case of test BM-3. The case of test BM-2 is not considered in this validation due to the complication caused by the change of loading configuration.

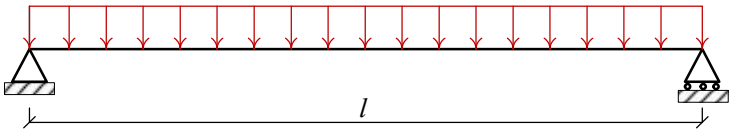

Figure 39: Loading and boundary conditions for the validation cases against experimental tests.

Figure 40 shows the comparison of moment-midspan displacement curves obtained from the experimental tests and from the numerical model. It can be seen from the figure that a good agreement between the two results was achieved for both experimental tests.

Figure 41 illustrates the comparison of slip distributions along the beam axis obtained from the experimental tests and from the numerical model for different levels of bending moment. M_u is the maximum force obtained from the flexural tests ($M_u = 1915$ kN. m for BM-1 and $M_u = 1720$ kN. m for BM-3). It can be observed that the slip distributions agree well between the results obtained from numerical model and from experiments for both cases (BM-1 and BM-3) until a load level of 80% of M_u. At the load level close to M_u, the difference between the two results become noticeable. However, when looking at the moment-slip curves (see Figure 42) for the slips at the extremities of the beams, the two curves correlate closely.

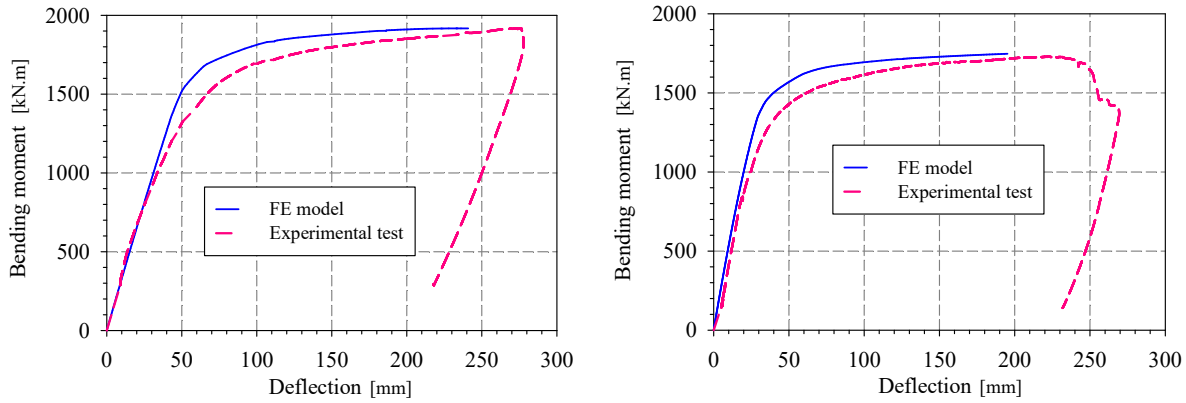

(a). Test BM-1.

(b). Test BM-3.

Figure 40: Comparison of moment-midspan displacement curves.

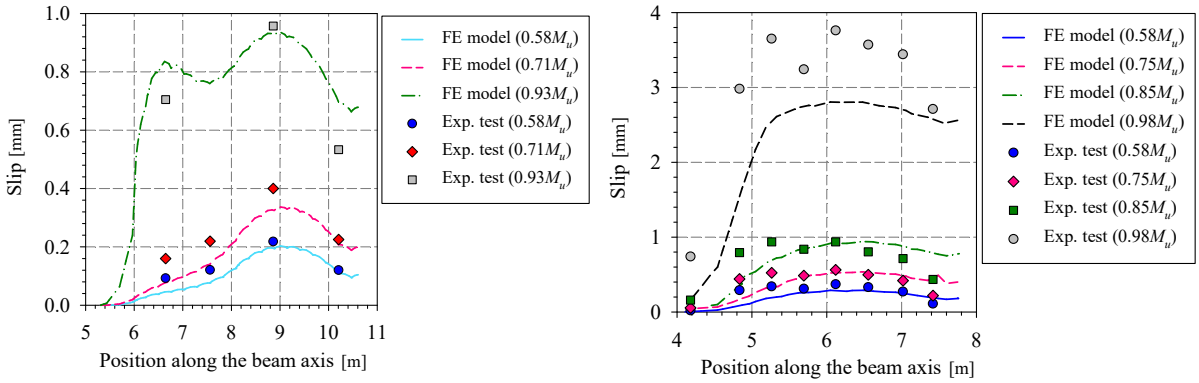

(a). Test BM-1

(b). Test BM-3

Figure 41: Comparison of slip distributions along the beam length.

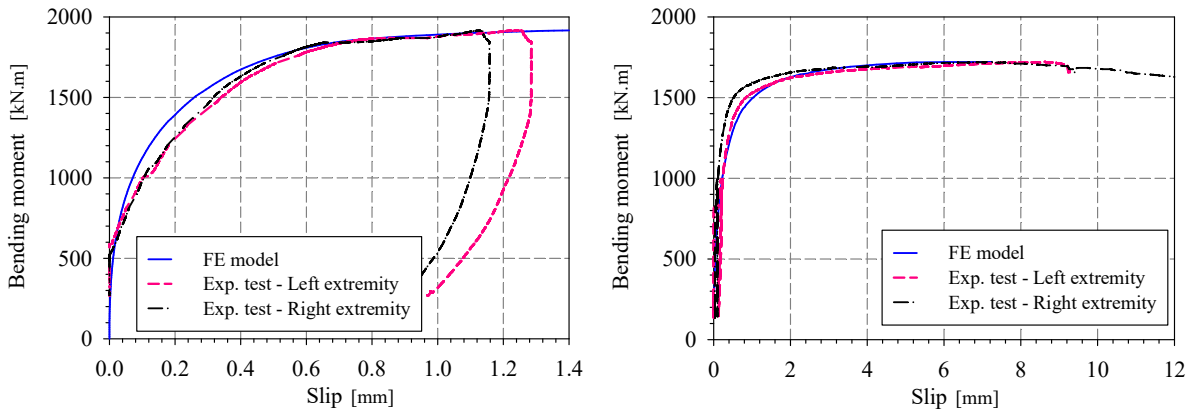

(a). Test BM-1. (b). Test BM-3.

Figure 42: Comparison of moment-slip curves at the extremity of the beam.

5.4.2 Extension of the validation of the analytical models

Once validated against the experimental results, the numerical model is used to compute in new configurations, in order to give more information over the consistency of the analytical models presented in section 4 for the definition of the resistance and of the bending stiffness of the USCB.

For the validation, two typical cases of beam span, i.e. 10 m and 20 m, are considered. For each case, two sections are chosen in order to cover the case where the neutral axis is found in the concrete slab and the one where the neutral axis is found in the concrete beam drop. All the four cases of the cross-section (P1-a, P1-b, P2-a and P2-b) are given in Figure 43 and Figure 44. The loading and boundary conditions are the same as presented in Figure 39.

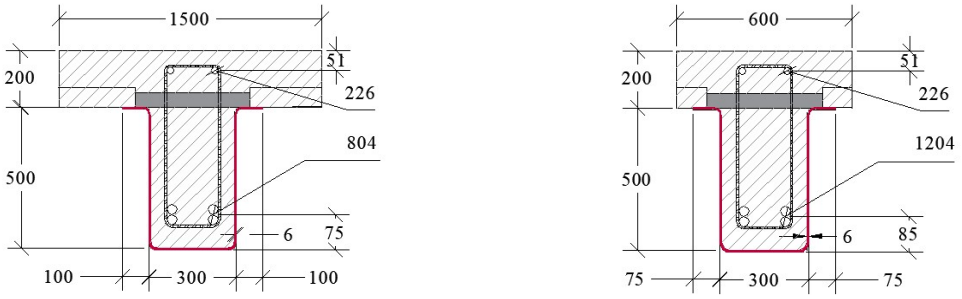

(a). Section P1-a. (b). Section P1-b.

Figure 43: Beam sections for a span of 10 m.

As the analytical approaches do not include the hardening effect of the materials, the elastic perfectly plastic constitutive relationship is used for steel elements in the numerical model. The properties for each material are given in Table 6.

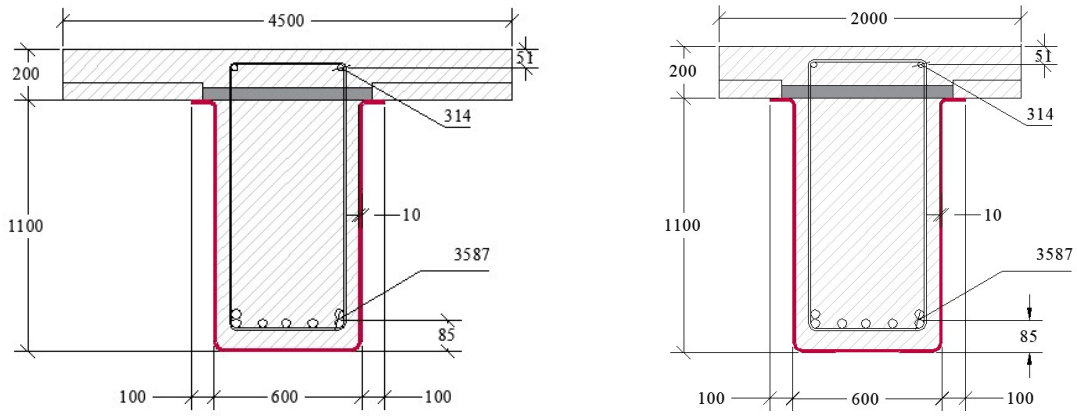

(a). Section P2-a. (b). Section P2-b.

Figure 44: Beam sections for a span of 20 m.

Table 6: Properties for each material.

U-shaped steel		Rebars		Concrete	
$f_{y,U}$ [MPa]	E_U [MPa]	$f_{y,R}$ [MPa]	E_R [MPa]	f_{cm} [MPa]	E_c [MPa]
235	210 000	435	210 000	16.67	25 645

The behaviour of the connector is modelled by the relationship provided in Eq. (43). In order to cover different values of the degree of shear connection, the resistance of the shear connection per linear meter is determined as follow:

$$p_{\eta,Rd} = n_l P_u = \eta \frac{V_{l,1}}{l/2} \tag{44}$$

where η is the degree of connection, taken between 0.5 and 1. $V_{l,1}$ is computed following Eq. (5). n_l is the number of shear connectors per meter length.

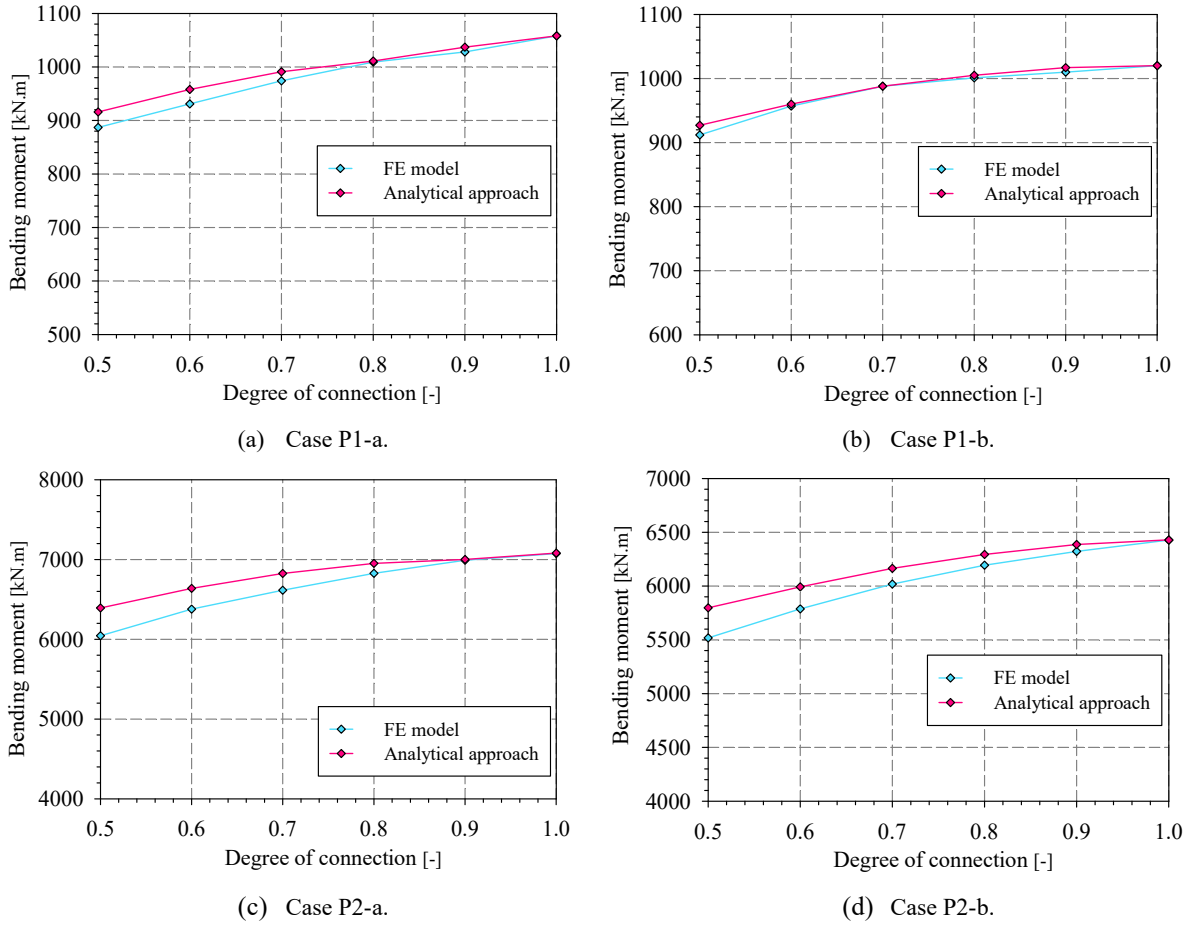

Figure 45: Comparison between the results obtained from analytical approach and from numerical model.

Figure 45 provides the comparison between the results of the bending moment capacity in function of the degree of shear connection (in a range between 0.5 and 1) obtained from the analytical approach adopted from Chen et al [4] and from the numerical model for each case of the study. It can be observed from the figure that a good agreement is obtained. The maximum difference for all the cases is six percent.

For each case, a ratio between the deflection of the beam with partial shear connection (δ_η) and the deflection of the beam with full shear connection (δ_1) is also computed using the analytical approaches of different norms (see Section 4.1.2) and using the numerical model at the serviceability load level (see Eq. (22)). Figure 46 shows the comparison of the evolution of the deflections in function of the degree of shear connection obtained from analytical approaches and from numerical model for each case of the study. In most of the cases, the ratios between the deflections obtained from the numerical model are smaller than the ones computed from the different approaches. The maximum difference between the results obtained from the British, the American and the Australian standards compared to the ones obtained from the numerical model are 35 percent, 7.5 percent and 8.5 percent, respectively. This once again shows the validity of the American and the Australian standards for estimating the flexural stiffness of the USCB and that the British standard is not suitable.

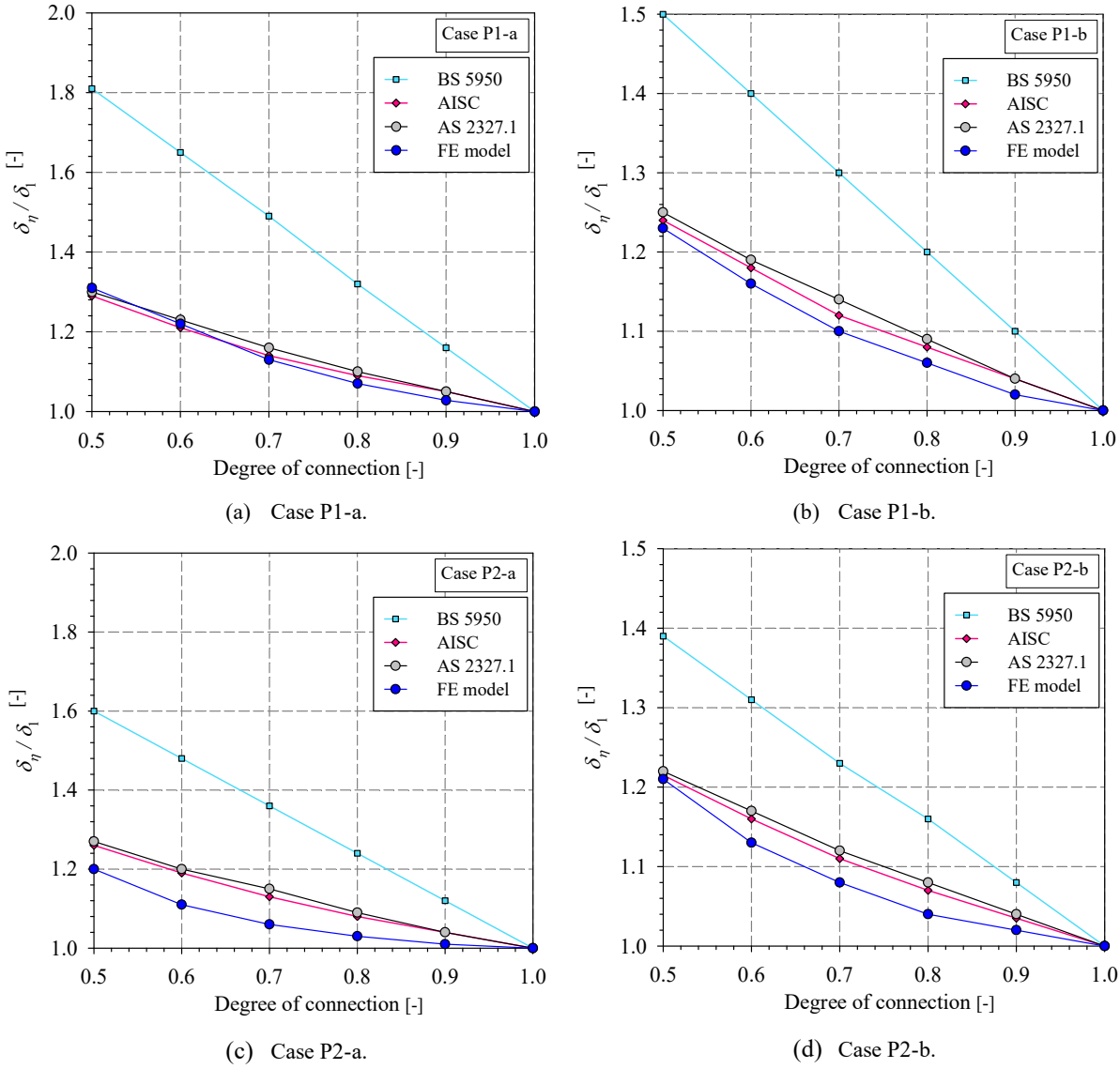

(a) Case P1-a. (b) Case P1-b.

(c) Case P2-a. (d) Case P2-b.

Figure 46: Comparison of the deflections of the beam obtained from analytical approach and from numerical model.

6. Parametrical study on the bending capacity and the flexural stiffness of the USCB

6.1 Description of the parametrical study

In this section, a parametrical study using the analytical approach described in Section 4.1.1 is carried out to evaluate the influence of different parameters such as the concrete strength (f_{ck}), the steel strength of U-shaped profile ($f_{y,U}$) and the degree of shear connection (η), on the bending resistance of the composite beam. The study uses three configurations of the beams, two of which are case P1-a and case P2-a with a beam span of 10 m and 20 m, respectively (see Figure 44). The third configuration P3 presents a beam span of 15 m with a cross-section as illustrated in Figure 47. These cases cover the field of use of the USCB. The degree of shear connection ranges from 0.5 to 1, and a strength class of S500B is used for the rebars. To investigate the influence of the strength of the U-shaped steel profile and the concrete strength on the maximum bending moment, three steel grades (S235, S275 and S355) and four concrete strengths (25 MPa, 30 MPa, 35 MPa and 40 MPa) are considered in this study.

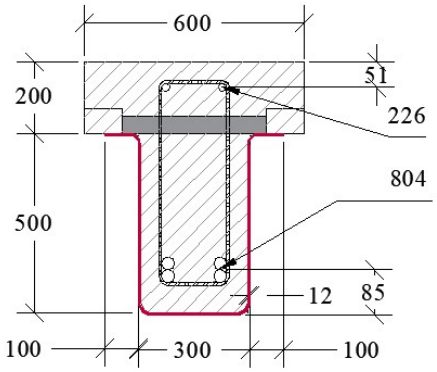

Figure 47: Section case P3.

6.2 *Influence of the parameters on the bending capacity of the USCB*

Figure 48, Figure 49 and Figure 50 illustrate the evolution of the bending moment as a function of the degree of shear connection for several values of steel strength $f_{y,U}$ and different values of concrete strength f_{ck} in the cases P1-a, P2-a and P3, respectively. Different line types are adopted for the various values of $f_{y,U}$ while several values in concrete strength are represented by different markers. In addition, to better quantify the influence of the yield strength of the U-shaped profile and the concrete strength, the following ratios are computed and presented in Table 7, Table 8 and Table 9 for the cases P1-a, P2-a and P3, respectively:

- $M_{pl,Rd,\eta} / M_{pl,Rd,\eta,f_{y,U,235}}$, being the ratio of the bending moment in each case to the one in the case with $f_{y,U}$ = 235MPa for the same concrete strength and the same degree of shear connection.
- $M_{pl,Rd,\eta} / M_{pl,Rd,\eta,f_{ck}25}$, being the ratio of the bending moment in each case to the one in the case with f_{ck} = 25MPa for the same steel strength of U-shaped profile and the same degree of shear connection.

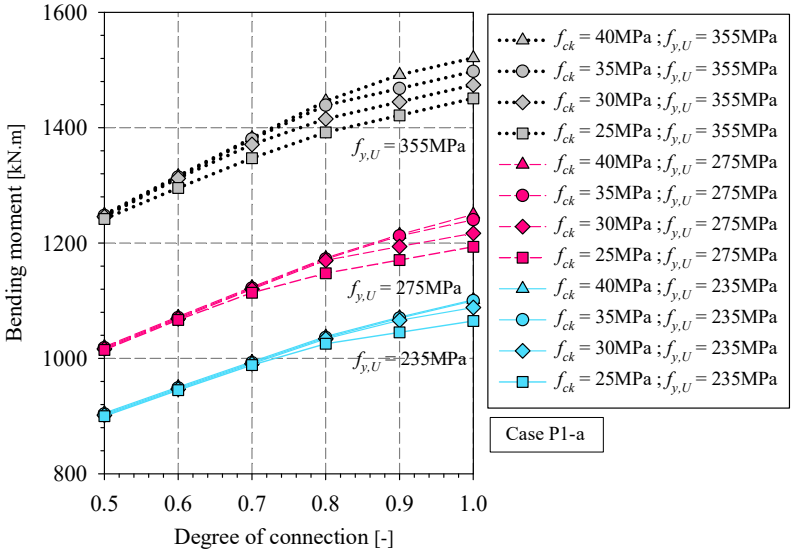

Figure 48: Evolution of the bending moment in function of the degree of connection for case P1-a.

Table 7: Statistical values of ratios $M_{pl,Rd,\eta}/M_{pl,Rd,\eta,f_{y,U,235}}$ and $M_{pl,Rd,\eta}/M_{pl,Rd,\eta,f_{ck}25}$ for case P1-a.

	$M_{pl,Rd,\eta}/M_{pl,Rd,\eta,f_{y,U,235}}$						$M_{pl,Rd,\eta}/M_{pl,Rd,\eta,f_{ck}25}$					
	$f_{y,U}$ = 235MPa		$f_{y,U}$ = 275MPa		$f_{y,U}$ = 355MPa		$f_{y,U}$ = 235MPa		$f_{y,U}$ = 275MPa		$f_{y,U}$ = 355MPa	
	Max. [%]	Min [%]	Max. [%]	Min [%]	Max. [%]	Min [%]	Max. [%]	Min [%]	Max. [%]	Min [%]	Max. [%]	Min [%]
f_{ck} = 25MPa	100	100	113	112	138	136	100	100	100	100	100	100
f_{ck} = 30MPa	100	100	113	112	139	135	102	100	102	100	102	100
f_{ck} = 35MPa	100	100	113	113	139	136	103	100	104	100	103	100
f_{ck} = 40MPa	100	100	113	113	139	138	103	101	105	100	105	100

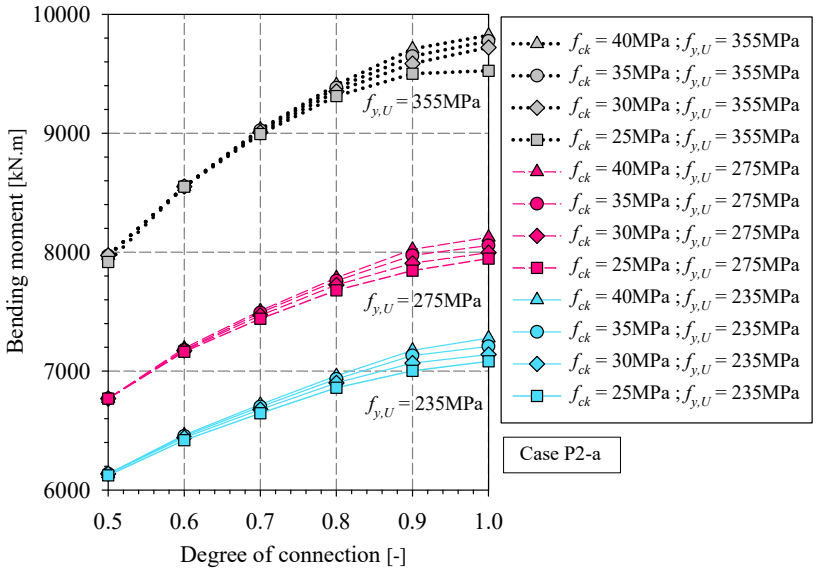

Figure 49: Evolution of the bending moment in function of the degree of connection for case P2-a.

640 Table 8: Statistical values of ratios $M_{pl,Rd,\eta}/M_{pl,Rd,\eta,f_{y,U,235}}$ and $M_{pl,Rd,\eta}/M_{pl,Rd,\eta,f_{ck}25}$ for case P2-a.

	$M_{pl,Rd,\eta}/M_{pl,Rd,\eta,f_{y,U,235}}$						$M_{pl,Rd,\eta}/M_{pl,Rd,\eta,f_{ck}25}$					
	$f_{y,U}$ = 235MPa		$f_{y,U}$ = 275MPa		$f_{y,U}$ = 355MPa		$f_{y,U}$ = 235MPa		$f_{y,U}$ = 275MPa		$f_{y,U}$ = 355MPa	
	Max. [%]	Min [%]	Max. [%]	Min [%]	Max. [%]	Min [%]	Max. [%]	Min [%]	Max. [%]	Min [%]	Max. [%]	Min [%]
f_{ck} = 25MPa	100	100	112	111	136	129	100	100	100	100	100	100
f_{ck} = 30MPa	100	100	112	110	136	130	101	100	101	100	102	100
f_{ck} = 35MPa	100	100	112	110	136	130	102	100	102	100	103	100
f_{ck} = 40MPa	100	100	112	110	135	130	103	100	102	100	103	100

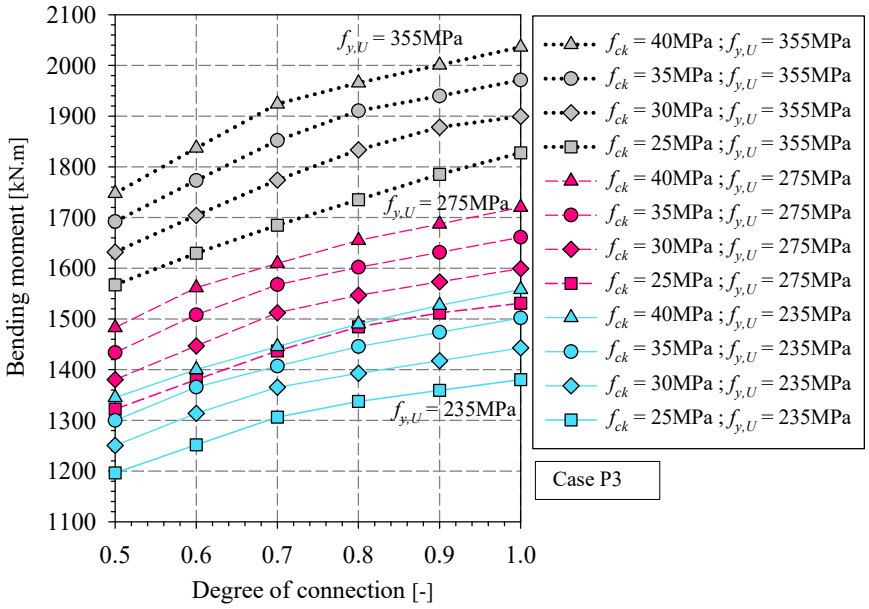

Figure 50: Evolution of the bending moment in function of the degree of connection for case P3.

Table 9: Statistical values of ratios $M_{pl,Rd,\eta}/M_{pl,Rd,\eta,f_{y,U,235}}$ and $M_{pl,Rd,\eta}/M_{pl,Rd,\eta,f_{ck}25}$ for case P3.

	$M_{pl,Rd,\eta}/M_{pl,Rd,\eta,f_{y,U,235}}$						$M_{pl,Rd,\eta}/M_{pl,Rd,\eta,f_{ck}25}$					
	$f_{y,U}$ = 235MPa		$f_{y,U}$ = 275MPa		$f_{y,U}$ = 355MPa		$f_{y,U}$ = 235MPa		$f_{y,U}$ = 275MPa		$f_{y,U}$ = 355MPa	
	Max. [%]	Min [%]	Max. [%]	Min [%]	Max. [%]	Min [%]	Max. [%]	Min [%]	Max. [%]	Min [%]	Max. [%]	Min [%]
f_{ck} = 25MPa	100	100	111	110	132	129	100	100	100	100	100	100
f_{ck} = 30MPa	100	100	111	110	132	130	105	104	105	104	106	104
f_{ck} = 35MPa	100	100	111	110	132	130	109	108	109	108	110	108
f_{ck} = 40MPa	100	100	112	110	133	130	113	111	113	111	114	111

The main observations are as follows:

- In the three cases, the higher steel strength of the U-shaped profile increases the bending capacity. As can be seen in the figures and the tables, a raise in yield strength ($f_{y,U}$) from 235 MPa to 275 MPa and from 235 MPa to 355 MPa leads to almost 13% and 40% gain of the bending capacity, respectively. Consequently, it can be concluded that it is efficient to increase the strength of the U-shaped steel profile when the design requires higher bending capacity of the USCB;
- In cases of beam configurations with the neutral axis in the concrete slab (Cases P1-a and P2-a), a small increase of bending capacity is obtained with the increase of the concrete strength, especially when the degree of shear connection is low. A maximum increase of bending capacity of around 5 percent is achieved between the cases with concrete strength of 25 MPa and 40 MPa;
- For Case P3 (neutral axis in the beam drop), the evolution of the bending moment is different from those in the cases P1-a and P2-a. An increase of bending capacity of around 5 percent when changing the

concrete strength from 25 MPa to 30 MPa, and of around 12 percent when changing the concrete strength from 25 MPa to 40 MPa;

Hence, the impact of the concrete strength on the bending capacity of the USCB is less important that of the steel strength of U-shaped profile. It would be preferable economically to increase the steel grade of the U-shaped profile than the concrete strength in order to improve the bending capacity of the USCB.

6.3 Influence of the parameters on the flexural stiffness of the USCB

Figure 51 shows the deflection ratio as a function of the degree of shear connection for several values of different values of concrete strength f_{ck} in the cases P1-a, P2-a and P3. In this figure, the deflection ratio $\delta_\eta / \delta_{1,C25}$ is the proportion between the deflection in each case and the deflection in the case with f_{ck} = 25 MPa and the degree of shear connection $\eta = 1$. From the figure, the following observations are made:

- For Cases P1-a and P3, an increase of the flexural stiffness of around 5 percent, 9 percent and 12 percent when changing the concrete strength from 25 MPa to 30 MPa, to 35 MPa and to 40 MPa, respectively;
- For Case P2-a, an increase of the flexural stiffness of around 2 percent, 6 percent and 9 percent when changing the concrete strength from 25 MPa to 30 MPa, to 35 MPa and to 40 MPa, respectively;
- In the three cases, by increasing the degree of shear connection from 0.5 to 1 helps to improve the flexural stiffness by about 26 percent.

In the economical point of view, it would not be interesting to increase the concrete class, as the improvement of the flexural stiffness is rather limited. It is more efficient to improve the degree of shear connection.

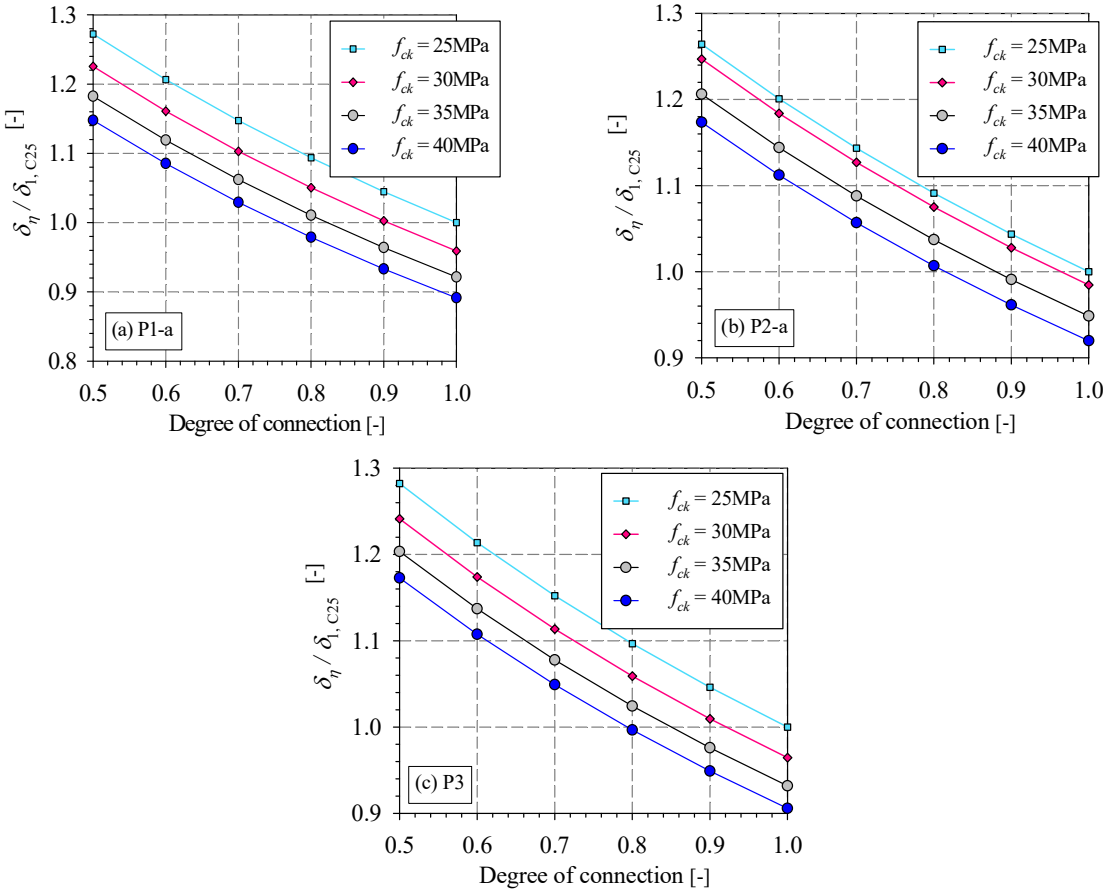

Figure 51: Deflection ratio in function of the degree of connection.

7. Conclusion

This paper presents a study on the influence of the partial shear connection on the behaviour of U-shaped steel concrete beam with L-shaped shear connectors under sagging bending moment. A series of three full-scale flexural tests of the USCB with a degree of shear connection ranging from 0.4 to 1 have been performed under sagging bending moment. The experimental tests were to determine the moment resisting capacity, the slip distribution along the length of the beam, the strain distribution on the cross-section, the ductility, and the failure mode. The bearing bending capacity obtained from the experimental results were compared to the values obtained from the full plastic analysis approach and from the simplified approach by Eurocode 4 [14]. The experimental results of flexural stiffness were also compared with the values obtained from the closed-form expressions given by British, Australian and American norms. A numerical model based on the two-layer beam element formulation taking into account the interlayer slips with continuous connection in a co-rotational framework was also adapted to determine the behaviour of the USCB and validated against experimental tests as well as against the analytical approaches. At last, a parametrical study was carried out in order to investigate the effect of selected parameters such as the

degree of shear connection, the concrete strength and the steel strength of U-shaped profile. The following outcomes can be extracted from this paper:

- The test results showed high ductility of the USCB with both full and partial shear connections. In the case of partial shear connections, the failure mode of the USCB was governed by the plastic buckling of the upper flanges of the U-shaped steel profile at the location of the critically loaded shear connectors.
- The full plastic analysis approach and the simplified approach by Eurocode 4 [14] are both applicable for determining the ultimate bending capacity of the USCB. However, the full plastic analysis approach gave more accurate results than the simplified approach provided in Eurocode 4 [14] when compared to the experimental results.
- American and Australian standards are more relevant to determine the flexural stiffness of the USCB, as compared to other discussed standards.
- The numerical model based on the two-layer beam element formulation taking into account the interlayer slips with continuous connection in a co-rotational framework was validated against experimental and analytical results.
- It would be economically preferable to increase the steel grade of the U-shaped steel profile than the concrete strength in order to improve the bending capacity of the USCB. On the other hand, to improve the flexural stiffness, it is possible to increase the concrete class and the degree of shear connection. The steel strength of the U-shaped profile has however no influence on the flexural stiffness of the USCB.

Acknowledgements

The work in this paper was developed in the framework of the CIFRE convention N° 2016/0256 between INSA Rennes and INGENOVA. The authors gratefully acknowledge financial support by the ANR (Agence Nationale de la Recherche, Paris) and INGENOVA with a grant number ANR-15-LCV2-0003 through the Labcom ANR B-HYBRID project.

References

[1] D. J. Oehlers, Composite profiled beams, Journal of Structural Engineering 119 (1993) 1085–1100.

[2] B. Uy, M. A. Bradford, Ductility of profiled composite beams: Part II experimental study, Journal of Structural Engineering 121 (1995) 876–882.

[3] S. Nakamura, Bending behaviour of composite girders with cold formed steel U section, Journal of Structural Engineering 128 (2002) 1169–1176.

[4] L.-H. Chen, S.-T. Li, H.-Y. Zhang, X.-F. Wu, Experimental study on mechanical performance of checkered steel-encased concrete composite beam, Journal of Constructional Steel Research 143 (2018) 223–232

[5] Y. Liu, L. Guo, B. Qu, S. Zang, Experimental investigation on the flexural behaviour of steel concrete composite beams with U-shaped steel girders and angle connectors, Engineering Structures 131 (2017) 492–502.

[6] J. Liu, Y. Zhao, Y. F. Chen, S. Xu, Y. Yang, Flexural behavior of rebar truss stiffened cold-formed U-shaped steel-concrete composite beams, Journal of Constructional Steel Research, 150 (2018) 175-185.

[7] P. Keo, C. Lepourry, H. Somja, F. Palas, Behaviour of a new shear connector for U-shaped steel-concrete hybrid beams, Journal of Constructional Steel Research 145 (2018) 153–166.

[8] R.P. Johnson, Composite Structures of Steel and Concrete, Volume 1 -Beams, slabs, columns, and frames for buildings, 1994.

[9] D.J. Oehlers, N. T. Nguyen, M. Ahmed & M.A. Bradford, Partial Interaction in Composite Steel and Concrete Beams with Full Shear Connection, Journal of Constructional Steel Research, vol 41, No 2/3, pp 235-248, 1997.

[10] J. Bujnak, Analyse globale de poutres mixtes acier béton : approche analytique et modélisation non-linéaire, Thèse de doctorat en génie civil, sous la direction de J.P. Muzeau, 2007.

[11] J. Nie, J. Fan, C.S. Cai, Experimental study of partially shear-connected composite beams with profiled sheeting. Engineering Structures, 30(2008), pp.1-12.

[12] E. Baran, C. Topkaya, Behavior of steel–concrete partially composite beams with channel type shear connectors. Journal of Constructional Steel Research, 97(2014), pp.69-78.

[13] A. Ozturk, E. Baran, C. Tort, Nonlinear Fiber Modeling of Steel-Concrete Partially Composite Beams with Channel Connectors. KSCE Journal of Civil Engineering, 23(5) (2019), pp.2227-2242.

[14] EN 1994, Eurocode 4: Design of composite steel and concrete structures, European Committee for Standardization, 2005.

[15] American Institute for Steel Construction (AISC). Load and resistance factor design specification for structural steel buildings. Chicago: AISC, 1999.

[16] C. Lepourry, P. Heng, H. Somja, N. Boissonnade, F. Palas, An Innovative Concrete-Steel Structural System for Long-Span Structure Allowing a Fast and Simple Erection, Structures, 21(2019), 55-74.

[17] NF EN12390-3, Testing harden concrete: Compressive Strength of Test Specimens, AFNOR - French standard institute, 2003.

[18] NF EN ISO 6892-1, Metallic materials - Tensile testing - Part 1 : method of test at room temperature, AFNOR - French standard institute, 2009.

[19] Aramis v8 manual basic, GOM mbH, Braunschweig (2015).

[20] EN 1992, Eurocode 2: Design of concrete structures, European Committee for Standardization, 2006.

[21] EN 1993, Eurocode 3: Design of steel structures, European Committee for Standardization, 2005.

[22] J.-M. Aribert, A. Lachal, “Formulation de la rupture par fatigue de connecteurs acier-béton pour des sollicitations de type sismique: Application aux assemblages,” Constr. métallique, vol. 39, no. 4, pp. 3–11.

[23] British Standards Institution. Structural use of steelwork in building, Part 3. Design in composite construction. Section 3.1, Code of practice for design of simple and continuous beams, BS 5950: Part 3: Section 3.1: 1990. London. 1990.

[24] American Institute of Steel Construction. Specification for structural steel buildings. Chicago (IL): AISC-360-10, American Institute of Steel Construction, 2010.

[25] Standards Association of Australia. Composite structures - simply supported beams. Australian Standard AS 2327.1-2003, Sydney, 2003.

[26] H. Ban, A. Bradford, Flexural behaviour of composite beams with high strength steel, Engineering Structures, vol 56, pp. 1130-1141, 2013.

[27] EN 1990, Eurocode 0: Basis of structural design, European Committee for Standardization, 2003.

[28] Q. H. Nguyen, Modélisation du comportement non-linéaire des poutres mixtes acier-béton avec prise en compte des effets différés. Ph.D. thesis. France: INSA de Rennes; 2009 [in French].

[29] J.-M. Battini, Q. H. Nguyen, M. Hjiaj, Non-linear finite element analysis of composite beams with interlayer slips, Computers and Structures, 87 (2009), pp 904-912.

[30] P. Keo, Q. H. Nguyen, H. Somja, M. Hjiaj, Geometrically nonlinear analysis of hybrid beam-column with several encased steel profiles in partial interaction, Engineering Structures, 100(2015), pp 66-78.

[31] M. Hjiaj, J.-M. Battini, Q. H. Nguyen, Large displacement analysis of shear deformable composite beams with interlayer slips, International Journal of Non-Linear Mechanics, 47 (2012), pp 895-904.

Annex: a simplified flowchart of the modelling process.